Benchmarking Validations for Dust Mobilization Models of GASFLOW Code

EFDA Reference: TW5-TSS-SEA 3.5 D4

Z. Xu, J. R. Travis, W. Breitung

Institut für Kern- und Energietechnik

August 2008

Forschungszentrum Karlsruhe

in der Helmholtz-Gemeinschaft

Wissenschaftliche Berichte

FZKA 7423

Benchmarking validations for dust mobilization models of GASFLOW code

EFDA reference: TW5-TSS-SEA 3.5 D4

Z. Xu, J.R. Travis[*], W. Breitung

Institut für Kern- und Energietechnik
*Ing. Büro DuBois-Pitzer-Travis, Offenbach
Programm Kernfusion

Abstract

Benchmarking validations for dust mobilization models of GASFLOW code

The governing equations of particle transport are defined and solved in the computational fluid dynamics code of GASFLOW. The particle motion model is based on the discrete Lagrangian approach being applicable to model the dust mobilization in the dilute dust / gas mixture, which is being expected to exist in the vacuum vessel of the ITER. A particle turbulent dispersion model and models of particle / boundary interactions, like rebound / deposition and entrainment, are defined as well. The deterministic particle trajectories obtained by GASFLOW simulations are verified against analytical solutions in both Cartesian and cylindrical systems. The stochastic particle dispersions caused by the turbulence in gas flow are compared between light and heavy particles in straight and curved ducts. Green's function method is applied to develop a bunch of theoretical solutions about particle concentration distributions in advective flows with different source / boundary conditions. The analytical solutions supply benchmarking verifications of the particle model of GASFLOW. Finally a graphite dust dispersion experiment is simulated by using GASFLOW. The comparison between the computed dust cloud developing process and the experimental one manifests that the particle model can produce the dust mobilization both qualitatively and quantitatively.

Kurzfassung

Validierung der GASFLOW-Staubmobilisierungsmodelle

Die Partikeltransportgleichungen werden im GASFLOW-Strömungsdynamikprogramm definiert und gelöst. Das Partikeltransportmodell beruht auf der Verwendung des diskreten Lagrange-Verfahrens zur Modellierung der im Vakuumbehälter von ITER im verdünnten Staub/Gas-Gemisch erwarteten Staubmobilisierung. Ebenso werden ein turbulentes Dispersionsmodell und Modelle für die Partikel/Grenzflächen-Wechselwirkungen, wie Abprall, Ablagerung und das Mitführen von Partikeln, definiert. Die mit Hilfe der GASFLOW-Simulationen ermittelten determini-stischen Partikeltrajektorien werden anhand der analytischen Lösungen in kartesischen und zylindrischen Systemen überprüft. Stochastische Partikeldispersionen, die auf die Turbulenz in der Gasströmung zurückzuführen sind, werden für leichte und schwere Partikel in geraden und gekrümmten Kanälen bestimmt und miteinander verglichen. Theoretische Lösungen für die Partikelkonzentrationsverteilungen in advektiven Strömungen werden unter verschiedenen Quellen-/Randbedingungen mit Hilfe der Green-Funktion ermittelt. Diese analytischen Lösungen dienen dann zur Verifizierung des GASFLOW-Partikelmodells. Abschließend wird ein Staubdisper-sionsexperiment mit Hilfe von GASFLOW simuliert. Der Vergleich von berechneter und experimenteller Staubwolkenentwicklung zeigt, dass das Partikelmodell die Staubmobilisierung sowohl qualitativ als auch quantitativ gut reproduziert.

CONTENTS

1. Introduction

The ITER Generic Site Safety Report (GSSR) showed the possibility of coexistence of combustible dusts, like carbon, beryllium and tungsten, and oxygen in the vacuum vessel when air ingression occurs in case of Loss of Vacuum Accidents (LOVA). It is obvious that the combustion of the dust accompanied by hydrogen- oxygen reactions presents a hazard to the whole fusion installation and the environment, through leakage of radiological elements like tritium and transient overpressures caused by possible explosions. As a first step, dust mobilization without chemical reactions should be understood. Therefore, it is necessary to conduct fundamental studies about the aerosol particle transport to understand and to predict theoretically the behaviors of the large amount of dust expected in the ITER facility.

The particle models including particle motion, diffusion, deposition/rebound and entrainment are developed and reviewed based on a computational fluid dynamics (CFD) computer code GASFLOW. The theoretical basis of the particle modeling in GASFLOW is the discrete Lagrangian approach. In the light of the approach, the particle motions follow the theorem of classic Newtonian mechanics. The method is applicable to dilute dust/fluid mixtures, in which the particle/fluid volume ratio is so small that the existence of particles does not influence the conveying flow at all. Such kind of dusts is exactly being expected in the ITER vacuum vessel.

The latest particle modeling is reviewed again in the report, although it is done already in the report of Joint Deliverable 1 (D1). Then the particle models are validated based on the series of theoretical and experimental benchmark test cases proposed in the report of Joint Deliverable 2 (D2). In order to validate the particle dispersion model, a mathematical tool of Green's function method (GFM) is applied to solve the multi-dimensional partial differential equations (PDE) about the dust mobilization, especially in the case that the aerosol particles are conveyed by an advective flow with dispersions. Thus a separated chapter is contributed to formulate the GFM and to apply it to validate the particle model of GASFLOW. Finally the whole work in the task is summarized.

2. Particle models

The particle behavior is governed by the local gas velocity field that exists after the final fluid dynamics task is performed in each

computational cycle. Each computational aerosol particle is initialized at specific physical mesh coordinates in the computational domain. The particle size and material properties are assigned to each particle. A location (x_p, y_p, z_p), velocity (u_p, v_p, w_p), diameter (d_p), and density (ρ_p) are stored for each particle.

2.1 Particle equations of motion

The fluid velocity components (u_g, v_g, w_g) at the particle location are computed from the fluid velocity components on the six faces of the cell that contains the particle. A linear interpolation is used in each direction, that is, a tri-linear interpolation. The equations of motion for a particle are as follows:

$$\frac{dx_p}{dt} = u_p, \tag{2-1-1}$$

$$\frac{dy_p}{dt} = v_p + \xi \frac{y_p}{x_p} u_p, \tag{2-1-2}$$

Drag force | Inertial acceleration in cylindrical system | Potential force

$$\frac{dz_p}{dt} = w_p, \tag{2-1-3}$$

$$\frac{du_p}{dt} = \eta \frac{3\pi\mu_g d_p}{m_p}(u_g - u_p) + (1-\eta)\frac{3}{4}C_D \frac{\rho_g}{\rho_p} \frac{(u_g - u_p)|\vec{U}_g - \vec{U}_p|}{d_p} + \xi \frac{v_p^2}{x_p} + g_x, \tag{2-1-4}$$

$$\frac{dv_p}{dt} = \eta \frac{3\pi\mu_g d_p}{m_p}(v_g - v_p) + (1-\eta)\frac{3}{4}C_D \frac{\rho_g}{\rho_p} \frac{(v_g - v_p)|\vec{U}_g - \vec{U}_p|}{d_p} - \xi \frac{u_p v_p}{x_p} + g_y, \tag{2-1-5}$$

$$\frac{dw_p}{dt} = \eta \frac{3\pi\mu_g d_p}{m_p}(w_g - w_p) + (1-\eta)\frac{3}{4}C_D \frac{\rho_g}{\rho_p} \frac{(w_g - w_p)|\vec{U}_g - \vec{U}_p|}{d_p} + g_z. \tag{2-1-6}$$

where, x_p, y_p, z_p the coordinates of particle location, cm; u_p, v_p, w_p the directional particle velocities, cm/s; u_g, v_g, w_g the directional fluid velocities, cm/s; g_x, g_y, g_z the directional gravities, cm/s^2; $\vec{U}_p, \vec{U}_g$ the velocity vectors of particle and fluid, respectively, cm/s; ρ_p, ρ_g the density of particle and fluid, respectively, g/cm^3; t the time, s; μ_g the gas dynamic viscosity, g/cms; m_p the particle mass, g; d_p the particle diameter, cm; η the option of Stokes flow (1 for Stokes flow and 0 for none Stokes flow); ξ the geometry factor (0 for

Cartesian coordinates and 1 for cylindrical coordinates); $\mathbf{C_D}$ the drag coefficient, defined as,

$$
\mathbf{C_D} = \begin{cases} \dfrac{24}{\mathbf{Re_p}}\left(1+\dfrac{\mathbf{Re_p^{\frac{2}{3}}}}{6}\right), & \text{if } \mathbf{Re_p} < 905, \\ 0.44, & \text{otherwise,} \end{cases}
\tag{2-1-7}
$$

where $\mathbf{Re_p}$, the particle Reynolds number, is

$$
\mathbf{Re_p} = \frac{\rho_g d_p \left|\vec{U}_g - \vec{U}_p\right|}{\mu_g}.
\tag{2-1-8}
$$

In Equation (2-1-4) through (2-1-6), the term $\dfrac{d}{dt}$ is the Lagrangian time derivative along the trajectory of the particle. The first two terms on the right-hand side are the acceleration resulting from fluid drag forces, where $\eta = 1$ or 0, $\eta = 1$ means the drag force satisfies the Stoke's law; otherwise, $\eta = 0$. The next term in Equation (2-1-4) and (2-1-5) accounts for inertial accelerations in a cylindrical coordinate system. The last term in each equation is the acceleration caused by potential body forces.

2.2 Particle diffusion

The particle velocity includes the mean velocity and the diffusion velocity, i.e.,

$$
\vec{U}_p = \vec{\bar{U}}_p + \vec{U}_{diff},
\tag{2-2-1}
$$

as shown in Figure 2-2-1 schematically.

The particle diffusion velocity represents the turbulent fluctuations on the mean motion, caused by the small scale turbulence in the gas flow or by particle concentration gradients. In case of homogeneous isotropic turbulence, the diffusion velocity, $\vec{U}_{diff}$, is formulated as,

$$
\vec{U}_{diff} = \sqrt{\frac{4\lambda}{\delta t}}[\pm\mathbf{erf}^{-1}(\zeta_1)\vec{i} \pm \mathbf{erf}^{-1}(\zeta_2)\vec{j} \pm \mathbf{erf}^{-1}(\zeta_3)\vec{k}],
\tag{2-2-2}
$$
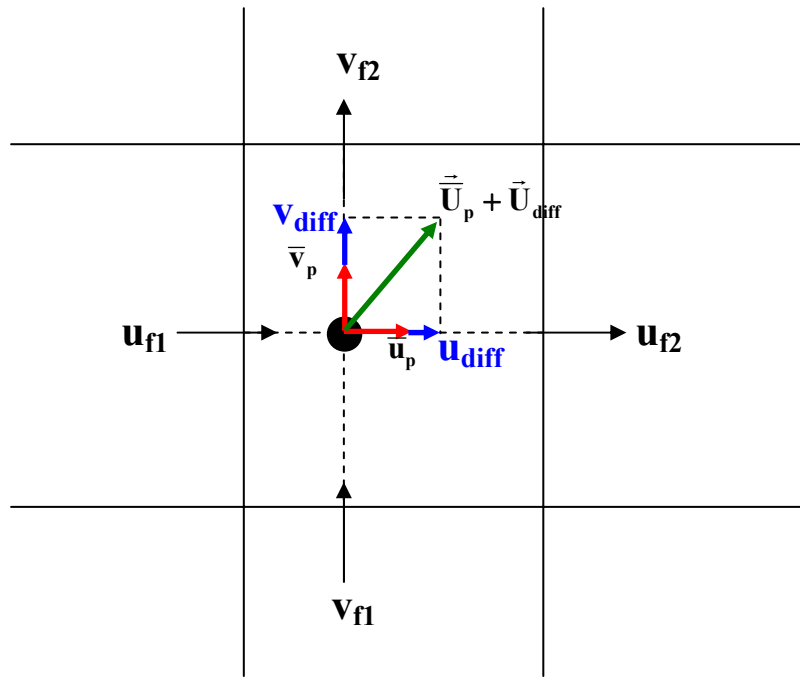
Figure 2-2-1 Particle diffusion velocity in two-dimensional numerical cell

where λ is the particle turbulent diffusion or dispersion coefficient, δt the particle time step for the numerical scheme, and $\zeta_1, \zeta_2, \zeta_3$ are random numbers between zero and one for the x, y, z directions, respectively. The direction of the fluctuation, i.e., the sign $\pm$ is also determined randomly. The statistical representation of the particle diffusion based on stochastic processes is mathematically equivalent to Fick's law of diffusion, and is actually a better approximation of particle diffusion in highly distorted flow and/or coarse mesh [1].

There are many approaches to model particle diffusion velocity described in the literatures. For the time being, either a constant particle diffusion coefficient λ or a functional value of λ is supplied for choice in the GASFLOW modeling. In the latter case, the diffusion coefficient varies with the local turbulence properties of the gas flow field. The turbulent particle diffusion coefficient is formulated as,

$$\lambda = \frac{\mu_{turb}}{\rho_g Sc_p} \cdot \frac{\tau_g}{\tau_g + \tau_p}, \qquad (2\text{-}2\text{-}3)$$

$$\tau_g = A_p \frac{k}{\varepsilon}, \qquad (2\text{-}2\text{-}4)$$

- 4 -

$$\frac{1}{\tau_p} = \eta \frac{3\pi\mu_g d_p}{m_p} + (1-\eta)\frac{3}{4}C_D \frac{\rho_g}{\rho_p} \frac{\left|\vec{U}_g - \vec{U}_p\right|}{d_p} , \qquad (2\text{-}2\text{-}5)$$

where μ_{turb} is the turbulent dynamic viscosity, g/cms, τ_p and τ_g are the relaxation times of particles and the fluid, respectively, in s, k, ε the turbulent kinetic energy (cm^2/s^2) and the dissipation rate (cm^2/s^3), respectively. The particle Schmidt number Sc_p and the A_p are input parameters in GASFLOW [2].

2.3 Deposition/rebound

When particle velocity components have been computed, the particle is moved in each of the coordinate directions. Particles hitting a solid boundary are specularly reflected or deposited on the surface.

A class of particles may all adhere, they may all bounce, or their behavior may be determined by the deposition/rebound model. The particle threshold bounce velocity, U_i^*, above which the particle may rebound, is determined in the model as follows:

$$U_i^* = \left[\frac{2E}{m_p}\left(\frac{1-e^2}{e^2}\right)\right]^{\frac{1}{2}} , \qquad (2\text{-}3\text{-}1)$$

where

$$E = \left(\frac{Ad_p}{12z_0}\right)\left[1+\left(\frac{A^2K^2d_p}{72z_0^7}\right)+\left(\frac{A^4K^4d_p^2}{72^2z_0^{14}}\right)\right]+\left(\frac{4\sqrt{2d_p}}{15K}\right)\left(\frac{A^2K^2d_p}{72z_0^6}\right)^{\frac{5}{2}} \qquad (2\text{-}3\text{-}2)$$

and A is the Hamaker constant, z_0 is the equilibrium separation between the particle sphere and a surface, d_p is the particle diameter, K is a function of mechanical properties, and m_p is the particle mass.

The critical rebound velocity, U_i^*, is the value of velocity for a 50% probability of bounce. The incident velocity window outside of which the particle either adheres or bounces is somewhat arbitrary, but plus or minus 50% of U_i^* is a reasonable assumption for this; that is, for $U_i < 0.5U_i^*$ the particle always adheres, and for $U_i > 1.5U_i^*$ the particle always bounces. When the velocity is in the range $0.5U_i^* < U_i < 1.5U_i^*$ the determination of whether or not specific

particles will bounce or adhere is made by generating a random number, α, with a value between 0 and 1, and testing for α as follows:

$$\alpha \leq \left[\frac{U_i - 0.5U_i^*}{U_i^*} \right]$$ (2-3-3)

When this condition is met, the particle bounces. The determination of deposition or rebounding is schematically shown in Figure 2-3-1.
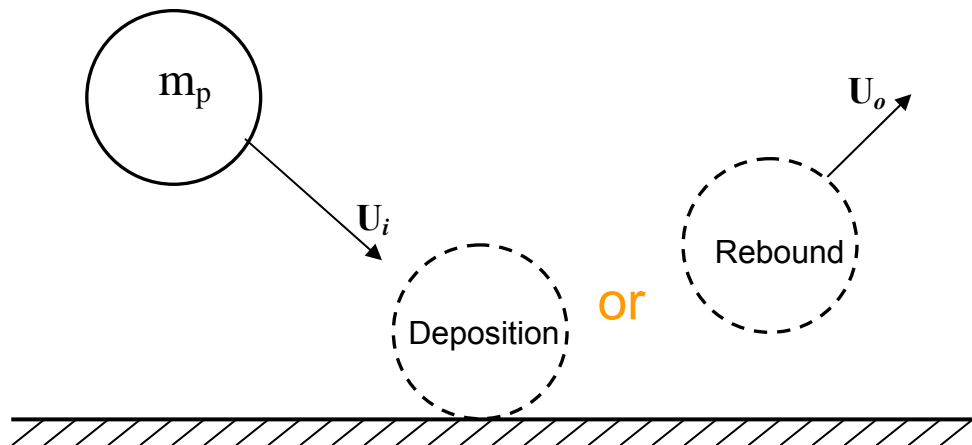
Figure 2-3-1 Scheme of particle deposition and rebound
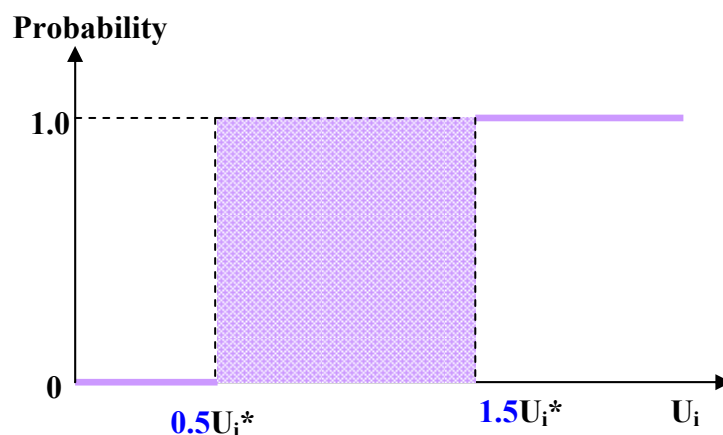

Figure 2-3-2 Probability of particle deposition and rebound

The experimentally observed trend is for the coefficient of restitution, e, to reach a maximum value at the threshold bounce velocity, and almost immediately the ratio of rebound velocity to incident velocity begins to decrease as the incident velocity increases. The following equation is used to model this behavior:

$$\mathbf{e} = \mathbf{e}_0 (0.60)^{\mathbf{exp}},$$ (2-3-4)

where

$$\mathbf{exp} = \frac{\mathbf{U_i} - \mathbf{U_i^*}}{10.0 \mathbf{U_i^*}},$$ (2-3-5)

and $\mathbf{e}_0$ is the coefficient of restitution at the threshold bounce velocity, as an input parameter.

Deposition is, in a real sense, a stochastic process that follows the general trend of the theoretical and empirical models developed and compared with available experimental data. Because of this, it is a reasonable assumption that some small, unknown percentage of the particles that impact a surface will adhere. To account for this, a percentage of all particles that impact a surface adhere. The percentage is chosen by an input parameter with a default value of 5%. The specific particles that adhere are randomly chosen, using the random number generator.

2.4 Entrainment

A single particle deposited on a surface will begin to move when the forces acting in the direction parallel to the surface are zero. These opposing forces are typically the fluid-drag force and the frictional force, which is the product of the normal forces and the coefficient of friction. For a horizontal surface as an example, the particle forces normal to the surface are adhesion, gravitational, buoyant and lift forces as shown in Figure 2-4-1; for vertical surfaces the gravitational and buoyant forces are tangential to the surface. A force balance equation of these surface and aerodynamic forces is iteratively solved by a Newton-Ralphson method to determine the minimum pickup velocity of each particle. This equation is,

$$\underbrace{C_D \frac{\pi}{8} d_p^2 \rho_g U_{gcp}^2}_{\text{Drag force,}} = f_s \left[\underbrace{\frac{\pi}{6} d_p^3 (\rho_p - \rho_g) g}_{\text{Sum of buoyancy and gravity,}} + \underbrace{\frac{A d_p}{12 z_0^2} \left(1 + \frac{A^2 K^2 d_p}{108 z_0^7}\right)}_{\text{Adhesive force,}} - \underbrace{1.615 U_{gcp} d_p^2 \sqrt{\nu \frac{\partial U_g}{\partial y}}}_{\text{Lift force}} \right],$$

Coefficient of friction

(2-4-1)

where the drag coefficient C_D is expressed in (2-1-7).

The vector $\mathbf{U}_{gcp}$ is the velocity of the gas at the center of the particle and is the computed particle threshold gas pickup velocity, $\mathbf{U}_{gpu0}$. Particle suspension is initiated when the velocity of the fluid flowing around the particle equals or exceeds this particle threshold suspension velocity.
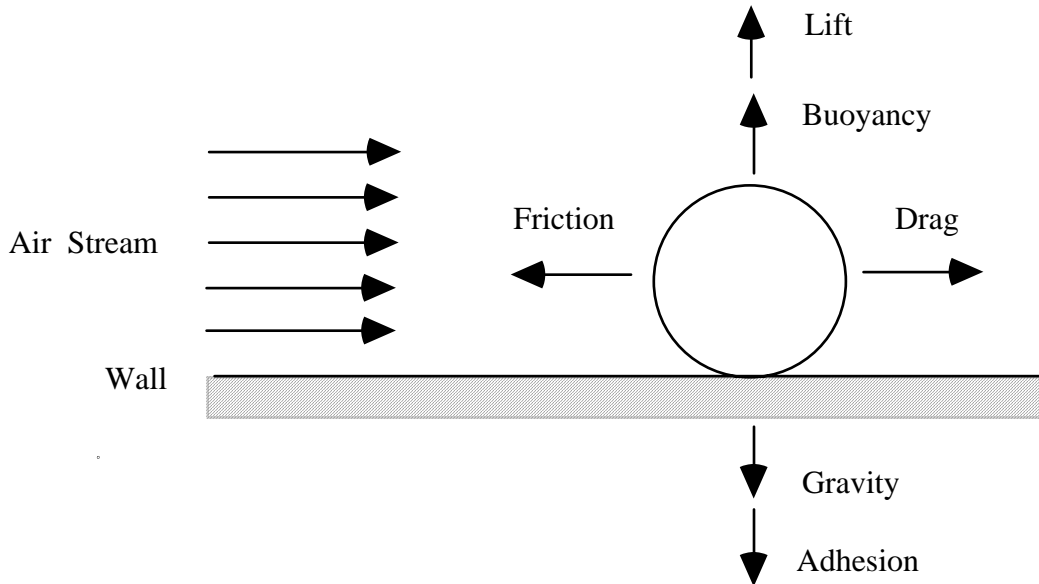
Figure 2-4-1 Forces acting on a single sphere at rest on a wall with a steady, fully developed turbulent flow

This model uses a force balance approach modified by the experimental data of Cabrejos and Klinzing [3]. After the threshold suspension velocity in each coordinate direction for each particle is computed, these velocities are adjusted by the experimental data to obtain a semi-empirical threshold velocity. The correlation is,

$$\mathbf{U}_{gpu} = \left(1.27\mathbf{Ar}^{-\frac{1}{3}} + 0.036\mathbf{Ar}^{\frac{1}{3}} + 0.45 \right)\left(0.7\mathbf{Ar}^{-\frac{1}{5}} + 1.0 \right)\mathbf{U}_{gpu0}, \qquad (2\text{-}4\text{-}2)$$

where the Archimedes number is

$$\mathbf{Ar} = \frac{\mathbf{g}}{\mathbf{v}_g^2}\frac{\left(\rho_p - \rho_g\right)}{\rho_g}\mathbf{d}_p^3. \qquad (2\text{-}4\text{-}3)$$

The semi-empirical threshold velocity component is computed for each particle for each coordinate direction.

The semi-empirical threshold velocity is used to test for particle entrainment. The orientation of the solid boundary on which the

particle is located in the computational mesh has been determined, and the information is stored in an array for each deposited particle. In addition, the velocity in each coordinate direction at the particle location has been computed and is stored. The determination of these velocities uses the law-of-the-wall equation to estimate these velocities at the particles, which are typically embedded in the viscous, inner sub-layer of the boundary layer. Again considering the stochastic behavior of particles, a probability of entrainment is computed. This is not based on experimental data but is solely an artifice to broaden the critical velocity at which particles will be suspended.

When $0.8\mathbf{U}_{gpu} \leq \mathbf{U}_{gcp} < \mathbf{U}_{gpu}$, the probability of entrainment is,

$$\mathbf{PRB}_{ntrn} = 4.0\left(\frac{\mathbf{U}_{gcp} - 0.8\mathbf{U}_{gpu}}{\mathbf{U}_{gpu}}\right). \qquad (2\text{-}4\text{-}4)$$

When $\mathbf{U}_{gcp} \geq \mathbf{U}_{gpu}$,

$$\mathbf{PRB}_{ntrn} = 0.8 + \left(\frac{\mathbf{U}_{gcp} - \mathbf{U}_{gpu}}{\mathbf{U}_{gpu}}\right). \qquad (2\text{-}4\text{-}5)$$

This gives an 80% probability of entrainment when the gas velocity at the particle location, $\mathbf{U}_{gcp}$, is equal to the semi-empirical threshold velocity, $\mathbf{U}_{gpu}$, and a 100% probability of entrainment when the velocity at the particle location is equal to or greater than 1.2 times the semi-empirical threshold velocity. The particle is never entrained when the gas velocity at the particle location is less than or equal to 0.8 times the semi-empirical threshold velocity. A random number, α, is generated and used to determine if the particle is actually entrained. When $\mathbf{PRB}_{ntrn} \geq \alpha$, the particle is entrained. In this case, the particle is assigned the local fluid velocity components parallel to the surface. The particle velocity component normal to the surface is set to zero. The particle is also moved to a point directly out from (normal to) the surface where the specific particle was located. The distance from the surface at which the particle is set is between one-half and one computational cell dimension. The exact location in this range is randomly chosen.
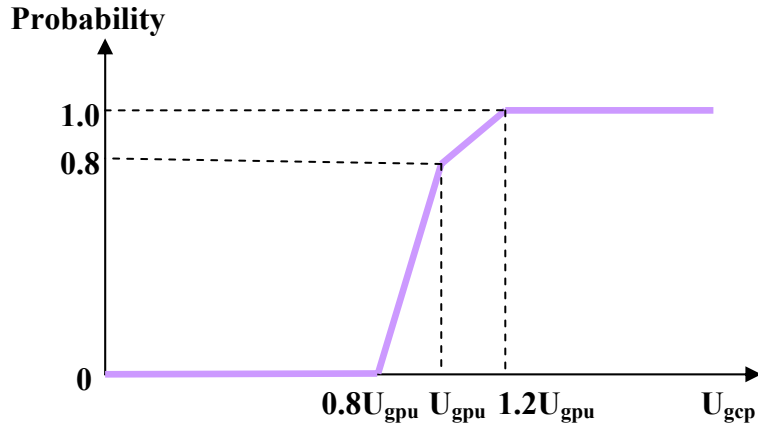
Figure 2-4-2 Probability of particle entrainment

2.5 Particle cloud model

The concept of the discrete computational *simulation* particle representing a multitude of *real* particles, all of which are located at the same point in space as the *simulation* particle, is extended in the particle cloud model. This model permits each *simulation* particle to represent a multitude of *real* particles that disperse as a Gaussian cloud. The density and size of the *real* particles in the cloud of particles are the same as the *simulation* particle with which the cloud is associated. The particle cloud density, ρ_{pc}, at a selected point that is a distance $\mathbf{r}$ from the cloud center is given by

$$\rho_{pc}(\mathbf{r},\mathbf{t}) = \mathbf{M}_{pc}\left(\frac{1}{(2\pi)^{\frac{3}{2}}\sigma^3}\right)e^{\frac{-\mathbf{r}^2}{2\sigma^2}}, \tag{2-5-1}$$

where

$$\sigma = \mathbf{r}_{pci} + \sqrt{2\mathbf{D}_{pc}\mathbf{t}}. \tag{2-5-2}$$

The term $\mathbf{M}_{pc}$ is the mass of the particle cloud, $\mathbf{D}_{pc}$ is the particle diffusion coefficient of the cloud, $\mathbf{r}_{pci}$ is the initial radius of the particle cloud, and $\mathbf{t}$ is the elapsed cloud growth time. The cloud density at any monitored point is determined by the summation of all density contributions of individual particle clouds at that point.
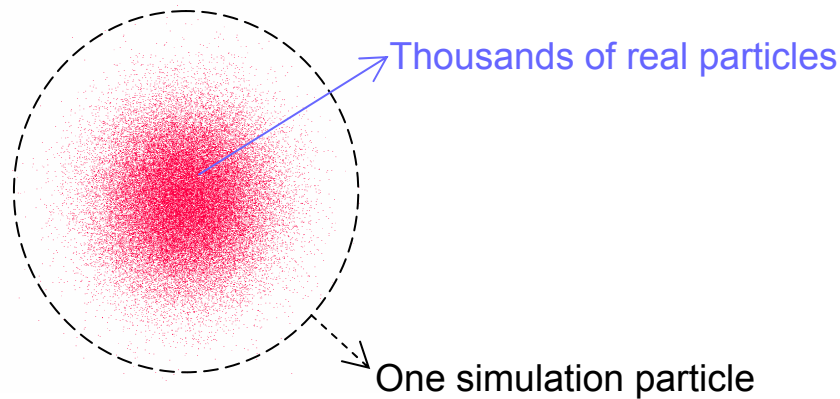
Figure 2-5-1 Particle cloud model

2.6 Numerical solution method

The basic procedure for advancing the particle transport solution through one increment of time, Δt, consists of four steps for each particle [4].

(1) Compute the fluid velocity at the particle location. This local fluid velocity, which is used to calculate the fluid drag force, has two parts: the velocity interpolated from the computed velocity field and a diffusion velocity.

(2) Compute intermediate particle velocities from explicit approximations of the momentum Equations (2-1-4) through (2-1-6) without fluid drag forces.

(3) Compute a new time-level particle velocity by iteratively adjusting the intermediate particle velocities to include the effects of the particle fluid drag forces.

(4) Move the particles to a new location using the average particle velocity for the time increment, Δt.

Following the transport of the particles, three additional phenomena are modeled.

(1) Deposit particles impacting a rigid surface, if criteria discussed in Section 2.3 are met.

(2) Entrain particles deposited on surfaces, if criteria discussed in Section 2.4 are met.

(3) Time-histories about *real* particle mass at selected locations in the computational domain can be detected by "monitors" and be plotted, if particle cloud model is switched on.

3. Particle model validations

3.1 Particle motion without dispersion

In order to verify the particle transport model only, the particle dispersion model is bypassed temporarily. Namely, the particles drift only with the accompany gas flow, but not disperse. Two test cases are designed to validate the performance of GASFLOW in the Cartesian and cylindrical coordinate systems, respectively.

3.1.1 Particle motion in Cartesian coordinate system

A two dimensional (2D) problem about particle drift in a uniform advection Stokes flow contained in a rectangular channel is chosen to verify the developed particle transport model in gravitational and non-gravitational environments, respectively. The Reynolds number $\mathbf{Re}_p$ based on the particle diameter is much less than unit in the cases, because the particle size is as small as microns and the fluid is highly viscous. Thus the drag force of the flow on the particles satisfies the Stoke's law. It means that $\eta = 1$ in the particle momentum equations.

3.1.1.1 Particle motion without potential force

The problem is schematically shown in Figure 3-1-1-1. The particle are injected vertically with an initial velocity of $\mathbf{V}_0$, into the horizontal uniformed flow in a velocity of $\mathbf{u}_0$.

The 2D governing equations are like,

$$\frac{d\mathbf{x}_p}{dt} = \mathbf{u}_p \, , \tag{3-1-1-1-1}$$

$$\frac{d\mathbf{y}_p}{dt} = \mathbf{v}_p \, , \tag{3-1-1-1-2}$$

$$\frac{d\mathbf{u}_p}{dt} = \frac{3\pi\mu_g d_p}{m_p}(\mathbf{u}_g - \mathbf{u}_p) \, , \tag{3-1-1-1-3}$$

$$\frac{d\mathbf{v}_p}{dt} = \frac{3\pi\mu_g d_p}{m_p}(\mathbf{v}_g - \mathbf{v}_p) \, , \tag{3-1-1-1-4}$$

u₀ → (arrows) **y**

Particle injection
velocity, **V₀**
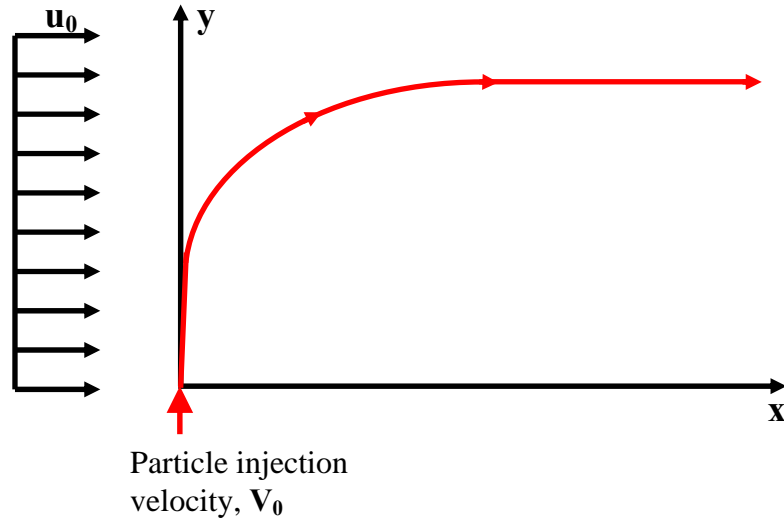
Figure 3-1-1-1 Benchmark of particle trajectory without gravity

with the initial conditions,

$$\mathbf{x_p}\mid_{t=0} = 0, \mathbf{y_p}\mid_{t=0} = 0, \mathbf{u_p}\mid_{t=0} = 0, \mathbf{v_p}\mid_{t=0} = \mathbf{V_0}, \qquad (3\text{-}1\text{-}1\text{-}1\text{-}5)$$

and in this case,

$$\mathbf{u_g} = \mathbf{u_0}, \mathbf{v_g} = 0. \qquad (3\text{-}1\text{-}1\text{-}1\text{-}6)$$

The analytical solution of the equations can be obtained by direct integration by parts,

$$\mathbf{x_p} = \mathbf{u_0}\left[\mathbf{t} - \frac{1 - \exp(-\Gamma t)}{\Gamma}\right], \qquad (3\text{-}1\text{-}1\text{-}1\text{-}7)$$

$$\mathbf{y_p} = \frac{\mathbf{V_0}}{\Gamma}\left[1 - \exp(-\Gamma t)\right], \qquad (3\text{-}1\text{-}1\text{-}1\text{-}8)$$

where, $\Gamma = 18\mu_g / \left(\rho_p \mathbf{d_p^2}\right).$ $\qquad (3\text{-}1\text{-}1\text{-}1\text{-}9)$

A numerical program is also developed outside of GASFLOW to solve the particle transport equations. The numerical solution is shown in Figure 3-1-1-2 together with the analytical solution and the GASFLOW simulation. In simulations, the parameters are given as, $\mu_g = 1.91 \times 10^{-4}$ g/cms, $\rho_p = 1$ g/cm^3, $\mathbf{d_p} = 5\mu m$, $\mathbf{u_0} = 2.5$ m/s, $\mathbf{V_0} = 25$ m/s.
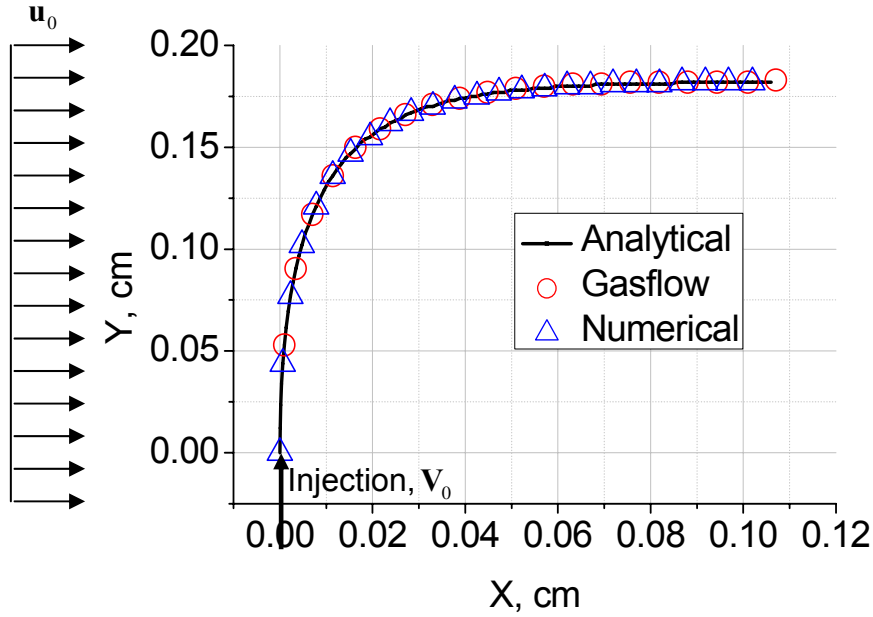
Figure 3-1-1-2 Trajectory comparison in Cartesian coordinate system without gravity

According to the figure, the three solutions agree with each other.

3.1.1.2 Particle motion with potential force

The only difference between this test case and the last case is that the particle/gas flow is in gravitational field. The governing equations and the solutions are given as follows,

$$\frac{d\mathbf{x}_p}{dt} = \mathbf{u}_p , \tag{3-1-1-2-1}$$

$$\frac{d\mathbf{y}_p}{dt} = \mathbf{v}_p , \tag{3-1-1-2-2}$$

$$\frac{d\mathbf{u}_p}{dt} = \frac{3\pi\mu_g d_p}{m_p}(\mathbf{u}_g - \mathbf{u}_p) + \mathbf{g}_x , \tag{3-1-1-2-3}$$

$$\frac{d\mathbf{v}_p}{dt} = \frac{3\pi\mu_g d_p}{m_p}(\mathbf{v}_g - \mathbf{v}_p) + \mathbf{g}_y , \tag{3-1-1-2-4}$$

with the initial conditions,

$$\mathbf{x}_p \mid_{t=0} = 0, \mathbf{y}_p \mid_{t=0} = 0, \mathbf{u}_p \mid_{t=0} = 0, \mathbf{v}_p \mid_{t=0} = \mathbf{V}_0 , \tag{3-1-1-2-5}$$

and in this case,

$$\mathbf{u}_g = \mathbf{u}_0, \mathbf{v}_g = 0, \mathbf{g}_x = 0. \tag{3-1-1-2-6}$$

The analytical solution of the equations can be obtained by direct integration by parts,

$$\mathbf{x}_p = \mathbf{u}_0 \left[\mathbf{t} - \frac{1 - \exp(-\Gamma \mathbf{t})}{\Gamma} \right], \tag{3-1-1-2-7}$$

$$\mathbf{y}_p = \left(\frac{\mathbf{V}_0}{\Gamma} - \frac{\mathbf{g}_y}{\Gamma^2} \right) [1 - \exp(-\Gamma \mathbf{t})] + \frac{\mathbf{g}_y}{\Gamma} \mathbf{t}, \tag{3-1-1-2-8}$$

where, $\Gamma = 18 \mu_g / \left(\rho_p \mathbf{d}_p^2 \right)$. \qquad (3-1-1-2-9)
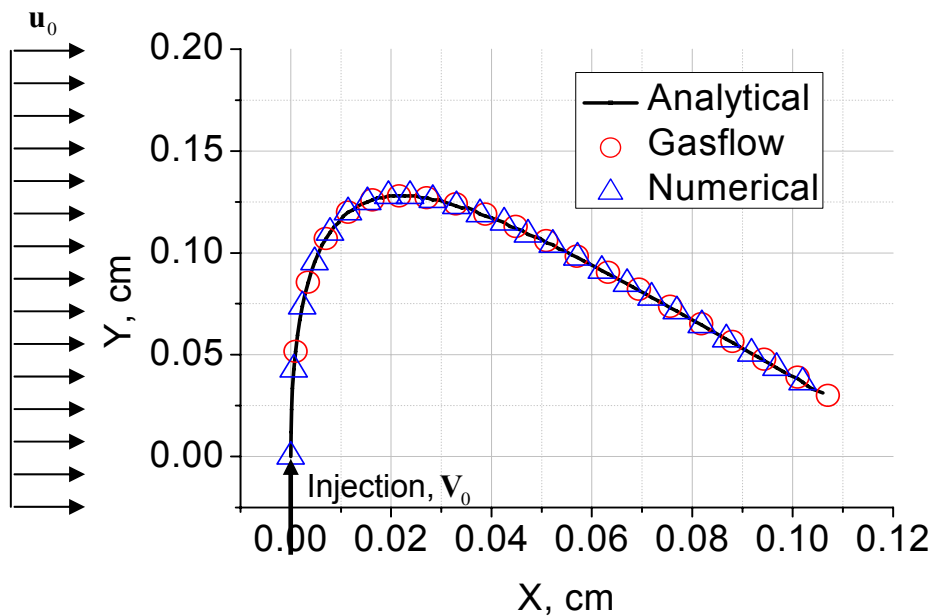

Figure 3-1-1-3 Trajectory comparison in Cartesian coordinate system with gravity

If $\mathbf{g}_y = -4.9 \times 10^5 \, \text{cm/s}^2$, the solutions are compared in Figure 3-1-1-3, which manifests that high consistencies are found between the numerical solution and the theory.

Based on the two test cases, it is validated that the particle transport equations are solved correctly in GASFLOW in the case of the Cartesian coordinate system.

3.1.2 Particle motion in cylindrical coordinate system
A particle motion problem in a cylindrical coordinate system was also designed to verify the model. A Stokes flow contained in a

180º curved duct has a fluid velocity distribution, in which the local velocity is proportional to the radial distance to the center of the duct, as shown in Figure 3-1-2-1. The particles are injected into the flow with an initial velocity equal to the local flow velocity, i.e., 3 cm/s. In Figure 3-1-2-1, apart from the particle trajectory simulated by GASFLOW, the blue triangle line is the solution obtained by directly solving the particle motion equations outside of GASFLOW. In this case, an elastic reflection boundary condition is applied when particles hit the rigid walls of the channel. The parameter settings about the particle models are the same as those in the last case of the Cartesian coordinate system. The agreement between the two trajectories demonstrates that the particle solver of GASFLOW works properly in the case of cylindrical coordinate system too.
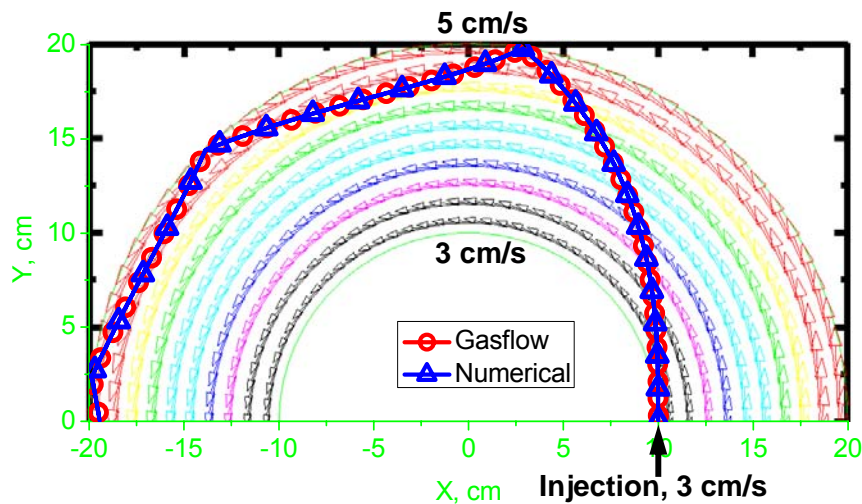

Figure 3-1-2-1 Trajectory comparison in a cylindrical coordinate system.

3.2 Particle mobilization with dispersion

Two cases of particle mobilization with dispersions are simulated by using GASFLOW in a straight duct and a curved duct, respectively.

3.2.1 Particle mobilization in two-dimensional straight duct

In this case the particles are released at the center line of a 2D straight channel containing a uniform advective flow. The particles are injected with an initial velocity identical to the flow velocity, 2 cm/s. Two parameters are adjusted to test the particle models, namely, the so-called Stokes coefficient α and the turbulent

diffusion coefficient of particle, λ. The Stokes coefficient is defined as,

$$\alpha = \frac{3\pi\mu_g d_p}{m_p},$$
(3-2-1-1)

which is inversely proportional to the particle mass if the particle diameter and the fluid viscosity keep constant. In the test case, the particle diffusion coefficient λ is handled as an adjustable constant to reflect the turbulent intensity. A bigger λ stands for stronger turbulence.

I. $\alpha = 1$ s^{-1} and $\lambda = 0.01$ cm^2/s

Twenty thousand of simulating particles with a diameter of 5 microns are injected into the advective air flow. The formed dust cloud is shown in Figure 3-2-1-1. It shows that the dust beam spreads a little because of the turbulence in the flow.

II. $\alpha = 1$ s^{-1} and $\lambda = 0.1$ cm^2/s

When the turbulence is intensified, i.e., λ is ten times higher than that of last case, the dust cloud is shown in Figure 3-2-1-2. It is obvious that the cloud spreads much more than that in Figure 3-2-1-1.

III. $\alpha = 0.1$ s^{-1} and $\lambda = 0.1$ cm^2/s

Comparing to the last case, if the only change is made to increase the particle mass ten times more, i.e., α ten times less, the dust cloud is shown in Figure 3-2-1-3. It indicates that the heavier particles are more difficult to diffuse, comparing to Figure 3-2-1-2.

The three test cases validate qualitatively that the particle diffusion model of GASFLOW can reproduce the physical diffusion of particles in the Cartesian coordinate system.
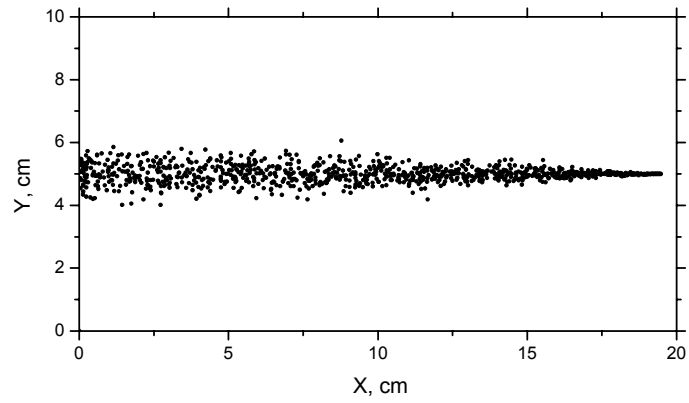
Figure 3-2-1-1 Dust cloud in straight duct with $\alpha = 1$ s^{-1} **and**
$\lambda = 0.01$ cm^2/s

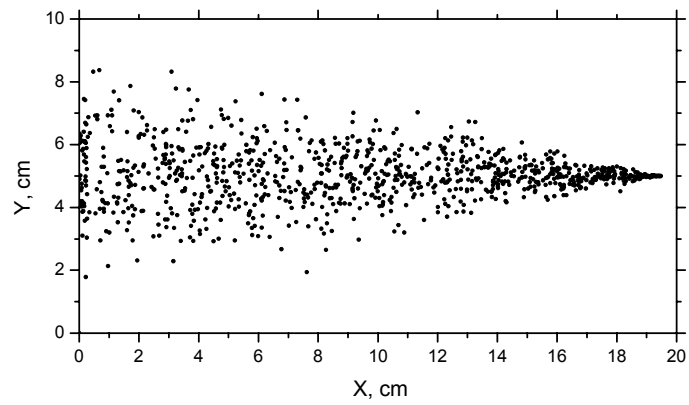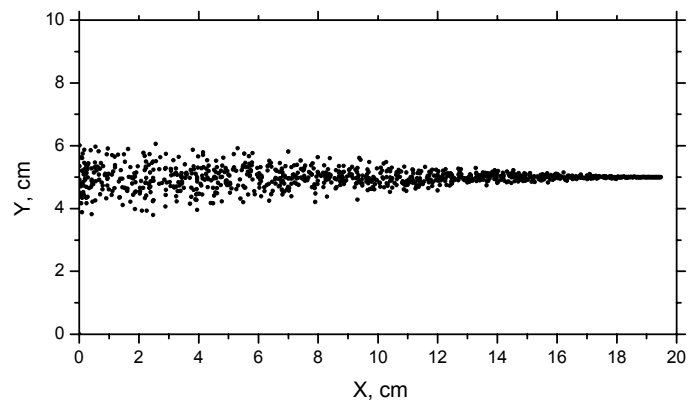**Figure 3-2-1-2 Dust cloud in straight duct with** $\alpha = 1$ s^{-1} **and**
$\lambda = 0.1$ cm^2/s

Figure 3-2-1-3 Dust cloud in straight duct with $\alpha = 0.1$ s^{-1} and $\lambda = 0.1$ cm^2/s

3.2.2 Particle mobilization in two-dimensional curved duct

The geometry of this test case is the same as that in Section 3.1.2. The advective flow is along the curved duct from the right end to the left. The flow velocity is proportional to the distance of the location to the center of the semi-circle, from 3 cm/s to 5 cm/s. Two classes of particle are injected simultaneously into the flow with an initial velocity of 3 cm/s from the left corner on the right end of the duct, as shown in Figure 3-2-2-1.
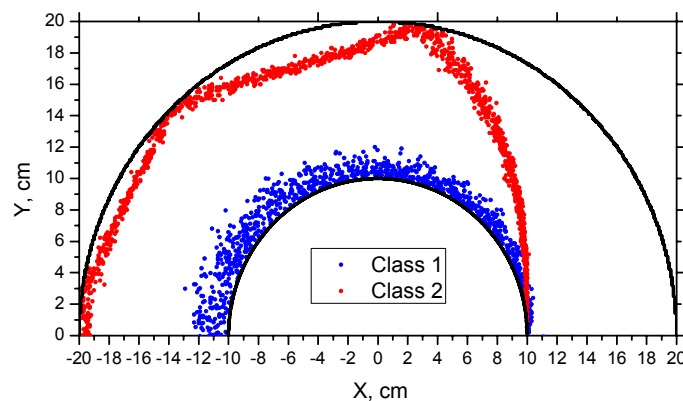
Figure 3-2-2-1 Separations of two particle classes in curved duct with advective flow

The two classes of particles share the same diameter of 5 microns, but class 2 is 100 times heavier than class 1. The Stoke's coefficients are 20 s^{-1} and 0.2 s^{-1} for the particle class 1 and 2, respectively. The particle diffusion coefficient is 0.05 cm^2/s. According the figure, it is clear that the relatively light particles are conveyed by the gas flow; but the heavier particles can penetrated the flow and hit on the wall of the duct, where, in this case, an elastic bounce is applied. It is interesting that the two classes of particles with different densities are separated at the left end of the duct. The test case validates comprehensively that the particle models of GASFLOW can predict basically the dust behaviors in the curved duct.

4. Green's function solutions and validations of dust models of GASFLOW

A series of particle mobilization problems are designed and simulated to validate the particle model of GASFLOW based on the theoretical solutions obtained by using the Green's function method (GFM). The particles are assumed to be released in an infinite advective gas flow. Then a dust cloud is formed owing to the advection and the diffusion. In theory the particle concentration in the cloud must be governed by the corresponding advection diffusion equation (ADE), which is a one- or multi-dimensional linear partial differential equation. The ADE can be solved and its analytical solution can be obtained by applying the GFM. Therefore this section is devoted to formulate the GFM in a succinct way and to apply the Green's function solutions to validate the dust model of GASFLOW.

4.1 Green's function method

The GFM is widely used to solve the partial differential equations encountered in engineering, for examples, in the literatures [5, 6, 7, 8, 9]. Some monographs [10, 11, 12] about Green's function can be referred if more details about the approach are desired.

4.1.1 Green's function solution

If the particle concentration is defined as $\mathbf{u}$, which is a function of the location $(\mathbf{x},\mathbf{y},\mathbf{z})$ and the time $\mathbf{t}$, and the advection velocity of the gas flow is $\mathbf{V}$, the particle diffusion coefficient $\mathbf{D}$, the particle source ϕ, then the particle advection diffusion problem in a three-dimensional (3D) domain is generally formulated as,

$$\mathbf{Lu} = \mathbf{u}_t + \mathbf{V}\mathbf{u}_x - \mathbf{D}(\mathbf{u}_{xx} + \mathbf{u}_{yy} + \mathbf{u}_{zz}) = \phi(\mathbf{x},\mathbf{y},\mathbf{z},\mathbf{t}) , \qquad (4\text{-}1\text{-}1\text{-}1a)$$

$$\mathbf{Bu} = \alpha\mathbf{u} + \beta\mathbf{u}_n = \mathbf{f} , \qquad (4\text{-}1\text{-}1\text{-}1b)$$

where, (4-1-1-1a) holds in a given domain R, which could be infinite or finite, and the boundary condition (4-1-1-1b) holds on the boundary B of the R. Here the advection direction is defined in the $\mathbf{x}$-direction without losing any general sense. The following steps are to describe the idea of the GFM and to apply it to solve the 3D ADE problem.

First, multiply Green's function $\mathbf{G}(\xi,\eta,\zeta,\tau)$ on both sides of (4-1-1-1a), and integrate by parts,

$$\iiint GLud\xi d\eta d\zeta d\tau = Boundary\_Terms + \iiint uL^*Gd\xi d\eta d\zeta d\tau, \quad (4\text{-}1\text{-}1\text{-}2)$$

where,

$$L = \frac{\partial}{\partial t} + V\frac{\partial}{\partial x} - D\nabla^2, \text{ and,} \quad (4\text{-}1\text{-}1\text{-}3)$$

$$L^* = -\frac{\partial}{\partial t} - V\frac{\partial}{\partial x} - D\nabla^2, \quad (4\text{-}1\text{-}1\text{-}4)$$

ξ, η, ζ, τ are dummy variables corresponding to x, y, z, t.

Then, in the light of the GFM, G is required to satisfy,

$$L^*G = \delta(\xi - x, \eta - y, \zeta - z, \tau - t), \quad (4\text{-}1\text{-}1\text{-}5)$$

with certain homogeneous boundary conditions that can make the unwelcome boundary terms in (4-1-1-2) vanish. They are unwelcome because they contain boundary values being not prescribed. Therefore the remaining terms are only those containing the prescribed boundary values. In terms of (4-1-1-1a), (4-1-1-2) and (4-1-1-5), the solution can be expressed as,

$$u(x, y, z, t) = \iiint G\phi d\xi d\eta d\zeta d\tau - Remaining\_Boundary\_Terms. \quad (4\text{-}1\text{-}1\text{-}6)$$

If the domain R is rectangular and is bounded in (x, y, z) space by,

$[x_1, x_2] \times [y_1, y_2] \times [z_1, z_2]$ or by $[\xi_1, \xi_2] \times [\eta_1, \eta_2] \times [\zeta_1, \zeta_2]$,

in (ξ, η, ζ) space, and if the time is define as $0 < t < \infty$, then the boundary terms in (4-1-1-6), created by integration by parts, can be expressed explicitly, i.e.,

$$u(x, y, z, t) = \int_0^t \int_{\zeta_1}^{\zeta_2} \int_{\eta_1}^{\eta_2} \int_{\xi_1}^{\xi_2} G\phi d\xi d\eta d\zeta d\tau + \int_{\zeta_1}^{\zeta_2} \int_{\eta_1}^{\eta_2} \int_{\xi_1}^{\xi_2} (Gu)\big|_{\tau=0} d\xi d\eta d\zeta +$$

$$+ \int_0^t \int_{\zeta_1}^{\zeta_2} \int_{\eta_1}^{\eta_2} [D(Gu_\xi - G_\xi u) - VGu]\big|_{\xi_1}^{\xi_2} d\eta d\zeta d\tau +$$

$$+ \int_0^t \int_{\zeta_1}^{\zeta_2} \int_{\xi_1}^{\xi_2} [D(Gu_\eta - G_\eta u)]\big|_{\eta_1}^{\eta_2} d\xi d\zeta d\tau +$$

$$+ \int_0^t \int_{\eta_1}^{\eta_2} \int_{\xi_1}^{\xi_2} [D(Gu_\zeta - G_\zeta u)] \Big|_{\zeta_1}^{\zeta_2} d\xi d\eta d\tau , \qquad (4\text{-}1\text{-}1\text{-}7)$$

where, both the welcome and unwelcome terms are included. (In the process of the integration by parts, a property of Green's function, $G\big|_{\tau=\infty} = 0$, is applied.) As mentioned, the unwelcome terms can be eliminated by applying the homogeneous boundary conditions of the Green's function.

The 3D Green's function equation (4-1-1-5) with the corresponding homogeneous boundary conditions can be solved directly by using image system based on inspection, integral transform, or by using eigenfunction method. However, the multi-dimensional Green's function solution can be created more easily based on the one-dimensional Green's functions, in the light of the so-called product rule of the GFM if the Cartesian coordinate system is adopted. If the directional 1D Green's functions in the Cartesian coordinate system are $X(\xi,\tau)$, $Y(\eta,\tau)$, $Z(\zeta,\tau)$, then the 3D Green's function must be, according to the product rule,

$$G(\xi,\eta,\zeta,\tau;x,y,z,t) = X(\xi,\tau;x,t)Y(\eta,\tau;y,t)Z(\zeta,\tau;z,t) . \qquad (4\text{-}1\text{-}1\text{-}8)$$

Once the Green's function is known, the particle concentration distribution in the advection diffusion problem can be obtained by the formula (4-1-1-7).

4.1.2 Green's functions of advection diffusion equation

If the concerned 3D domain is infinite and the advection is assumed to be along the x-axis without losing a general sense, the directional Green's functions are directly given here,

$$X(\xi,\tau) = \frac{H(t-\tau)}{\sqrt{4\pi D(t-\tau)}} \exp\left[-\frac{[\xi - x + V(t-\tau)]^2}{4D(t-\tau)}\right], \qquad (4\text{-}1\text{-}2\text{-}1)$$

$$X(\xi,\tau) = \frac{H(t-\tau)}{\sqrt{4\pi D(t-\tau)}} \exp\left[-\frac{(\xi - x)^2}{4D(t-\tau)}\right], \text{ if } V = 0 , \qquad (4\text{-}1\text{-}2\text{-}1')$$

$$Y(\eta,\tau) = \frac{H(t-\tau)}{\sqrt{4\pi D(t-\tau)}} \exp\left[-\frac{(\eta - y)^2}{4D(t-\tau)}\right], \qquad (4\text{-}1\text{-}2\text{-}2)$$

$$Z(\zeta,\tau) = \frac{H(t-\tau)}{\sqrt{4\pi D(t-\tau)}} \exp\left[-\frac{(\zeta - z)^2}{4D(t-\tau)}\right]. \qquad (4\text{-}1\text{-}2\text{-}3)$$

The 1D Green's functions supply the building blocks for the 3D Green's function, as already indicated in (4-1-1-8). The detailed procedure to obtain the Green's functions can be referred to [13].

4.2 Particle model validations based on Green's function solutions

In the test cases, the particles are released from a point, line, area or volume source into a stagnant or advective gas flow in a 3D infinite domain. The particle concentrations in the dust clouds are compared between the theoretical solutions and the GASFLOW simulations.

4.2.1 Point source in stagnant flow

4.2.1.1 Instantaneous point source

Mathematically, a Dirac delta function is applied to formulate the instantaneous particle release as a point source term with a constant coefficient to stand for the strength of the particle source. It can be assumed that the particles are released instantaneously at $t = 0$, and from the very center (origin) of an infinite 3D cube. The problem is formulated as,

$$\mathbf{u_t} - \mathbf{D(u_{xx} + u_{yy} + u_{zz})} = \mathbf{Q_3}\delta(\mathbf{x,y,z,t}), \; -\infty < \mathbf{x,y,z} < \infty, \; 0 < \mathbf{t} < \infty, \quad (4\text{-}2\text{-}1\text{-}1)$$

where $\mathbf{Q_3}$ is the total number of the released particles, or called "source strength". By applying the GFM, and noting the properties of delta function and the product rule about Green's functions, the solution can be expressed as,

$$\mathbf{u(x,y,z,t)} = \mathbf{Q_3} \int_0^t \int_{-\infty}^\infty \int_{-\infty}^\infty \int_{-\infty}^\infty \mathbf{G}(\xi,\eta,\zeta,\tau;\mathbf{x,y,z,t})\delta(\xi,\eta,\zeta,\tau)\mathbf{d}\xi\mathbf{d}\eta\mathbf{d}\zeta\mathbf{d}\tau =$$

$$= \mathbf{Q_3} \int_0^t \left[\int_{-\infty}^\infty \mathbf{X}(\xi,\tau;\mathbf{x,t})\delta(\xi)\mathbf{d}\xi \right]\left[\int_{-\infty}^\infty \mathbf{Y}(\eta,\tau;\mathbf{y,t})\delta(\eta)\mathbf{d}\eta \right]\left[\int_{-\infty}^\infty \mathbf{Z}(\zeta,\tau;\mathbf{z,t})\delta(\zeta)\mathbf{d}\zeta \right]\delta(\tau)\mathbf{d}\tau =$$

$$= \mathbf{Q_3} \int_0^t \mathbf{X}(0,\tau;\mathbf{x,t})\mathbf{Y}(0,\tau;\mathbf{y,t})\mathbf{Z}(0,\tau;\mathbf{z,t})\delta(\tau)\mathbf{d}\tau = \mathbf{Q_3}\mathbf{X}(0,0;\mathbf{x,t})\mathbf{Y}(0,0;\mathbf{y,t})\mathbf{Z}(0,0;\mathbf{z,t}),$$

$$(4\text{-}2\text{-}1\text{-}2)$$

where $\mathbf{X,Y,Z}$ stand for the directional Green's functions. By substituting the Green's functions, the solution can be obtained explicitly,

$$u(x,y,z,t) = Q_3 \left(\frac{1}{\sqrt{4\pi Dt}} \right)^3 \exp\left(-\frac{x^2}{4Dt} \right) \cdot \exp\left(-\frac{y^2}{4Dt} \right) \cdot \exp\left(-\frac{z^2}{4Dt} \right). \quad (4\text{-}2\text{-}1\text{-}3)$$

If the distance to the origin is denoted as r, the above formula can be reduced as, by noting that $r^2 = x^2 + y^2 + z^2$,

$$u(r,t) = \frac{Q_3}{\sqrt{(4\pi Dt)^3}} \exp\left(-\frac{r^2}{4Dt} \right), \quad (4\text{-}2\text{-}1\text{-}4)$$

where, $t \neq 0$.

The diffusion problem is simulated numerically by using GASFLOW. The computational results are compared with the above theoretical solutions in Figure 4-2-1-1. In the GASFLOW simulations, the key parameters are specified as follows: the particle diameter, $d_p = 5 \times 10^{-4}$ cm, the particle density, $\rho_p = 1\,g/cm^3$, the gas density $\rho_g = 1.179 \times 10^{-3}\,g/cm^3$, the gas dynamic viscosity, $\mu_g = 10^{-2}$ g/cms, thus, the particle Reynolds number $Re_p = \rho_g d_p |\vec{U}_g - \vec{U}_p| / \mu_g \ll 1$, where $\vec{U}_g, \vec{U}_p$ denote the velocities of the gas and the particle, respectively. In this case, the drag force of the conveying gas on the tiny particles satisfies the Stoke's law, and the Stoke's coefficient $\alpha_s = 18\mu_g /(\rho_p d_p^2) = 7.2 \times 10^5\,s^{-1}$. The particle diffusion coefficient is specified as $D = 0.1$ cm^2/s. The particle sample number is specified as 4×10^6. The particle concentration is defined as the particle number in unit volume. The normalized particle concentration is the particle concentration divided by the total particle number in the problem. Accordingly, the Q_3 in the Green's function solution is assumed to be equal to unit for normalization. The cell size is 0.1 cm in the simulation.

According to Figure 4-2-1-1, the particle concentrations are in Gaussian distributions with decaying amplitudes on time, as expected in view of physics. Good agreements are obtained between the analytical solutions and the simulations. In (b), some random deviations exist between the simulation points and the theoretical curve. However they are completely statistical effects, which should vanish if the particle sample number is sufficiently big. It can be concluded that the diffusion model of GASFLOW can work properly in case of diffusion from instantaneous sources in stagnant flows.
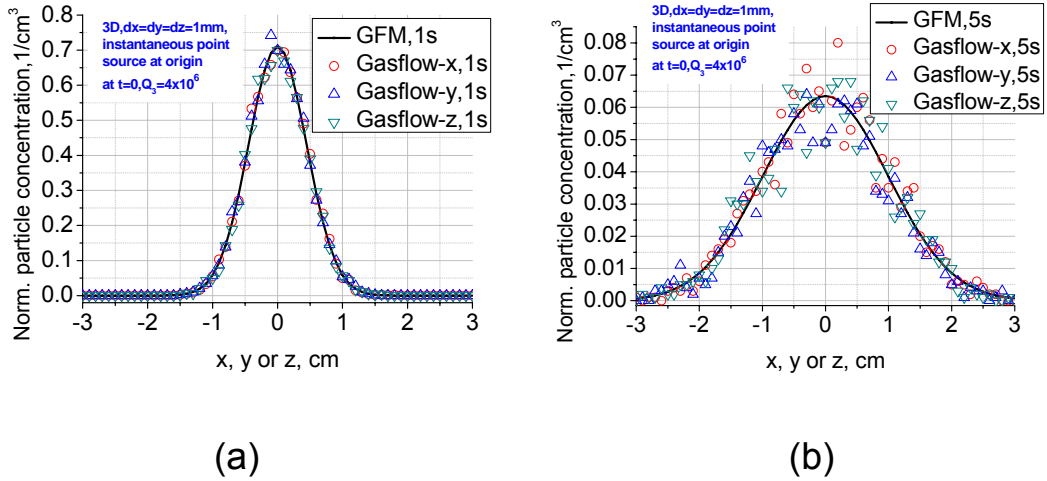
(a)   (b)

Figure 4-2-1-1 Particle diffusion from instantaneous point source in quiescent flow

4.2.1.2 Continuous point source

In case of continuous point source, let's take the 3D problem as an example to show how to create the Green's function solution. The formulation of the diffusion problem is described as,

$$\mathbf{u_t} - \mathbf{D}(\mathbf{u_{xx}} + \mathbf{u_{yy}} + \mathbf{u_{zz}}) = \mathbf{q_3}\delta(\mathbf{x,y,z}), \ -\infty < \mathbf{x,y,z} < \infty, \ 0 < \mathbf{t} < \infty. \qquad (4\text{-}2\text{-}1\text{-}5)$$

Based on the GFM, the solution should be in the form of,

$$\mathbf{u(x,y,z,t)} = \mathbf{q_3}\int_0^t \int_{-\infty}^{\infty}\int_{-\infty}^{\infty}\int_{-\infty}^{\infty} \mathbf{G}(\xi,\eta,\zeta,\tau;\mathbf{x,y,z,t})\delta(\xi,\eta,\zeta)\mathbf{d\xi d\eta d\zeta d\tau} =$$

$$= \mathbf{q_3}\int_0^t \left[\int_{-\infty}^{\infty}\mathbf{X}(\xi,\tau;\mathbf{x,t})\delta(\xi)\mathbf{d\xi}\right]\left[\int_{-\infty}^{\infty}\mathbf{Y}(\eta,\tau;\mathbf{y,t})\delta(\eta)\mathbf{d\eta}\right]\left[\int_{-\infty}^{\infty}\mathbf{Z}(\zeta,\tau;\mathbf{z,t})\delta(\zeta)\mathbf{d\zeta}\right]\mathbf{d\tau} =$$

$$= \mathbf{q_3}\int_0^t \mathbf{X}(0,\tau;\mathbf{x,t})\mathbf{Y}(0,\tau;\mathbf{y,t})\mathbf{Z}(0,\tau;\mathbf{z,t})\mathbf{d\tau}. \qquad (4\text{-}2\text{-}1\text{-}6)$$

The directional Green's functions are the same as in the instantaneous case. By substituting them into the above expression, we have,

$$\mathbf{u(x,y,z,t)} = \mathbf{q_3}\int_0^t \left(\frac{1}{\sqrt{4\pi\mathbf{D(t-\tau)}}}\right)^3 \exp\left[-\frac{\mathbf{x^2 + y^2 + z^2}}{4\mathbf{D(t-\tau)}}\right]\mathbf{d\tau}.$$

If the distance to the origin is defined as $\mathbf{r}$, by considering the property about convolution, we have,

$$u(x,y,z,t) = q_3 \int_0^t \frac{1}{\sqrt{(4\pi D\tau)^3}} \exp\left(-\frac{r^2}{4D\tau}\right) d\tau = \frac{q_3}{4\pi D|r|} \mathrm{erfc}\left(\frac{|r|}{\sqrt{4Dt}}\right), \qquad (4\text{-}2\text{-}1\text{-}7)$$

where $r^2 = x^2 + y^2 + z^2 \neq 0$ and $t \neq 0$. The q_3 stands for the released particle number per unit time.

The Green's function solution (4-2-1-7) is represented as solid lines in Figure 4-2-1-2. The q_3 is specified as one for normalization. The diffusion problem with the continuous point source is simulated by using GASFLOW. The parameters about the continuous sources are specified as: the total particle number 9.6×10^5, the total injection time 4s, the injection interval time 2.5×10^{-4} s. The other parameters are the same as the case of the instantaneous source.
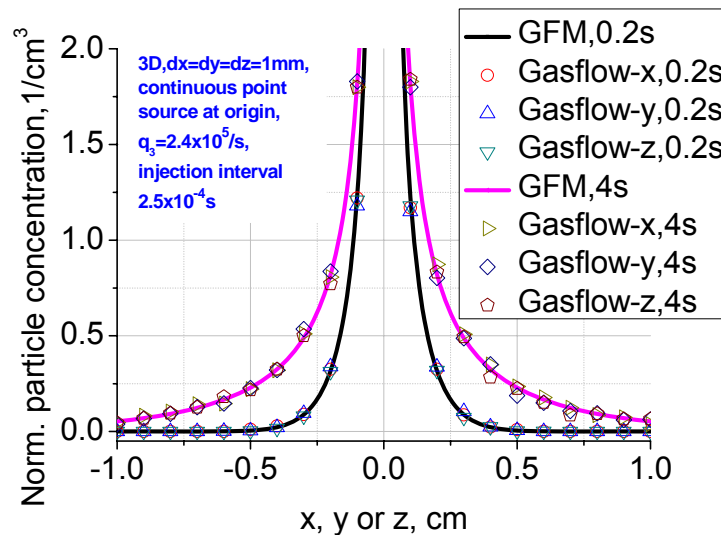

Figure 4-2-1-2 Particle diffusion from continuous point source in quiescent flow

Figure 4-2-1-2 manifests a good consistency about the particle distributions between the Green's function solution and the GASFLOW simulation. It verifies that the model about the continuous particle source in GASFLOW performs in a proper manner. It is worth to mention that, the particle concentration at the origin is infinite theoretically. The distribution at the vicinity of the origin is not of interest to be concerned in reality, as can be seen in the figure.

4.2.2 Point source in advective flow

This subsection is contributed to solve or to simulate the diffusion from an instantaneous or continuous point source to a uniform advective flow. From here on, the advective flow velocity is assumed to be equal to $V = 2$ cm/s as an example, if no additional words are given.

4.2.2.1 Instantaneous point source

The particles are released only once at the time $t = 0$ s, then they are transported by the accompanying advective gas flow and start to diffuse. The mathematical expressions for the advection diffusion problems are similar to those in the case of the stagnant flow in Section 4.2.1, except the advection term,

$$\mathbf{u_t} + \mathbf{V u_x} - \mathbf{D(u_{xx} + u_{yy} + u_{zz})} = \mathbf{Q_3 \delta(x,y,z,t)}, \ -\infty < \mathbf{x,y,z} < \infty, \ 0 < \mathbf{t} < \infty,$$

$$(4\text{-}2\text{-}2\text{-}1)$$

where the $\mathbf{u}$ denotes the particle concentration. The expressions of the solutions are also similar to those in the case of the stagnant flow, except that the Green's function in $\mathbf{x}$-direction (advection direction) is replaced by the advective Green's function. By the replacement, the solution can be obtained as,

$$\mathbf{u(x,y,z,t)} = \frac{\mathbf{Q_3}}{\sqrt{(4\pi \mathbf{Dt})^3}} \mathbf{exp}\left[-\frac{\mathbf{(x - Vt)^2 + y^2 + z^2}}{4\mathbf{Dt}} \right]. \qquad (4\text{-}2\text{-}2\text{-}2)$$

If $V = 2$ cm/s, $D = 0.1$ cm^2/s and $Q_3 = 1$ for normalization, the theoretical particle concentrations along the x-axis at different times are shown in Figure 4-2-2-1 as solid lines. It presents propagating Gaussian distributions along the x-direction and with decaying amplitudes on time, clearly due to the advective flow and the diffusion of the particles themselves. Accordingly the GASFLOW simulations are performed and the results are shown as symbols in Figure 4-2-2-1. The specifications about particles are the same as in Section 4.2.1. The released particle number is 10^6. It is obvious that the GASFLOW models reproduce the particle behaviors in a way following the analytical solutions.
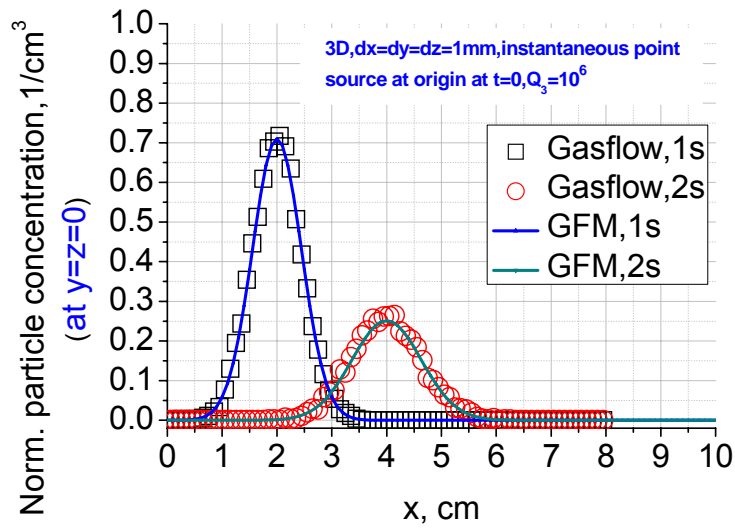
Figure 4-2-2-1 Particle diffusion from instantaneous point source in advective flow

4.2.2.2 Continuous point source

By applying the GFM, the 3D theoretical particle concentrations caused by continuous point sources in infinite domains with advective flows can be simply obtained as,

$$u(x,y,z,t) = \int_0^t \frac{q_3}{\sqrt{(4\pi D\tau)^3}} \exp\left[-\frac{(x-V\tau)^2 + y^2 + z^2}{4D\tau}\right] d\tau,$$
(4-2-2-3)

where q_3 is the particle release rate. The comparisons between the GFM solutions and the GASFLOW simulations are presented in Figure 4-2-2-2. In the simulations the continuous sources are defined as: the total particle number is 10^6 and the injection interval time 2.5×10^{-4} s, the total injection time is 2 s. The other parameters are the same as the previous cases. The numerical simulations agree well with the corresponding Green's function solutions according to the figure, which also shows that, a minor part of particles diffuse from the origin (release place) backward to the upstream while the major are transported away along the advection direction. The concentration in the neighborhood of the origin is not shown. It is not concerned and is infinite at the origin theoretically.
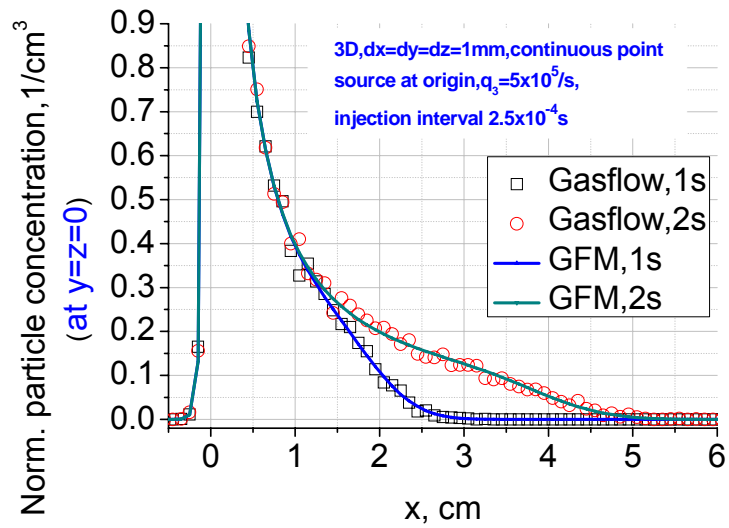
Figure 4-2-2-2 Particle diffusion from continuous point source in advective flow

4.2.3 Line source in three-dimensional advective flow

Two kinds of line sources are considered. One is in a transverse direction, the other in the advection direction, as shown in Figure 4-2-3-1.
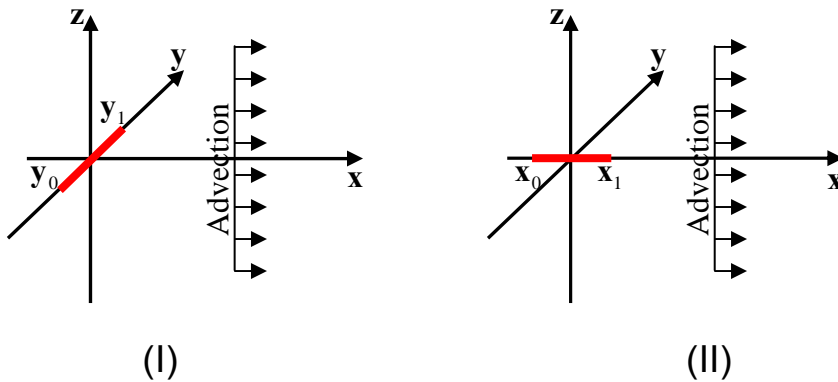

(I)   (II)

Figure 4-2-3-1 Two cases of line sources in infinite three-dimensional domain

4.2.3.1 Line source in transverse direction

By using a two-dimensional delta function, the mathematical equation of the particle concentration is formulated as,

$$\mathbf{u_t} + \mathbf{Vu_x} - \mathbf{D(u_{xx} + u_{yy} + u_{zz})} = \begin{cases} \mathbf{q_1\delta(x,z)}, & \text{if} \quad \mathbf{y \in [y_0, y_1]}, \\ \mathbf{0}, & \text{otherwise}, \end{cases} \qquad (4\text{-}2\text{-}3\text{-}1)$$

where $-\infty < x, y, z < \infty$, $0 < t < \infty$. In terms of the GFM, Green's functions are like building blocks, and the higher dimensional solutions can be created easily on the basis of lower dimensional ones. The 3D solution can be obtained simply by using the product rule and by utilizing the property of delta function,

$$u(x,y,z,t) = \int_0^t q_1 X(0,\tau;x,t) \int_{y_0}^{y_1} Y(\eta,\tau;y,t) d\eta Z(0,\tau;z,t) d\tau .$$
(4-2-3-2)

By bringing the Green's functions into the above equality and making a little simplification, the solution becomes,

$$u(x,y,z,t) = \int_0^t \frac{q_1}{8\pi D\tau} \exp\left[-\frac{(x-V\tau)^2+z^2}{4D\tau}\right]\left[\mathrm{erfc}\left(\frac{y-y_1}{\sqrt{4D\tau}}\right)-\mathrm{erfc}\left(\frac{y-y_0}{\sqrt{4D\tau}}\right)\right]d\tau .$$
(4-2-3-3)

The normalized solution and the numerical simulation are presented in Figure 4-2-3-2 for comparison, where $y_0 = -0.5$ cm and $y_1 = 0.5$ cm. It is obvious that GASFLOW can reproduce numerically the particle diffusion in a good way.
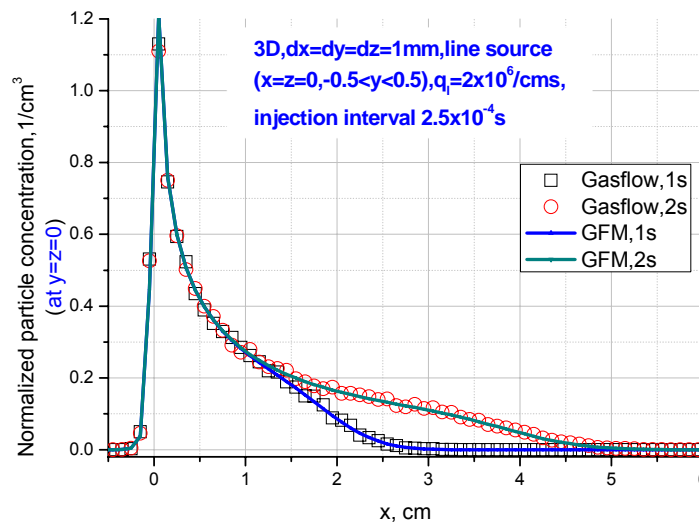

Figure 4-2-3-2 Advection diffusion from continuous particle line source distributed in transverse (y) direction in three-dimensional domain

4.2.3.2 Line source in advection direction
The equation and its solution are listed here for completeness.

$$u_t + Vu_x - D(u_{xx} + u_{yy} + u_{zz}) = \begin{cases} q_l\delta(y,z), & \text{if} \quad x \in [x_0, x_1], \\ 0, & \text{otherwise}, \end{cases} \qquad (4\text{-}2\text{-}3\text{-}4)$$

where $-\infty < x, y, z < \infty$, $0 < t < \infty$. The solution is,

$$u(x,y,z,t) = \int_0^t \frac{q_l}{8\pi D\tau}\left[\text{erfc}\left(\frac{x - V\tau - x_1}{\sqrt{4D\tau}}\right) - \text{erfc}\left(\frac{x - V\tau - x_0}{\sqrt{4D\tau}}\right)\right]\exp\left[-\frac{y^2 + z^2}{4D\tau}\right]d\tau .$$

$$(4\text{-}2\text{-}3\text{-}5)$$

If $x_0 = -0.5$ cm and $x_1 = 0.5$ cm, the theoretical curves and the GASFLOW simulation points are shown in Figure 4-2-3-3, where the concentrations distribute long the line of $y = z = 0.1$ cm instead of the x-axis. According to the figure, the simulating points fit the analytical curves in a satisfactory way.
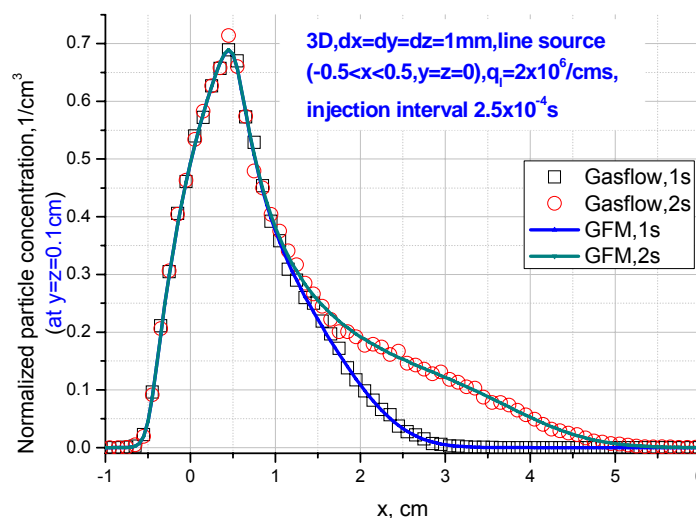

Figure 4-2-3-3 Advection diffusion from continuous particle line source distributed in advection (x) direction in three-dimensional domain

4.2.4 Area source in three-dimensional advective flow

Two cases of area sources are studied in 3D domain, as shown in Figure 4-2-4-1, depending on the spatial relationship between the area and the advection direction.
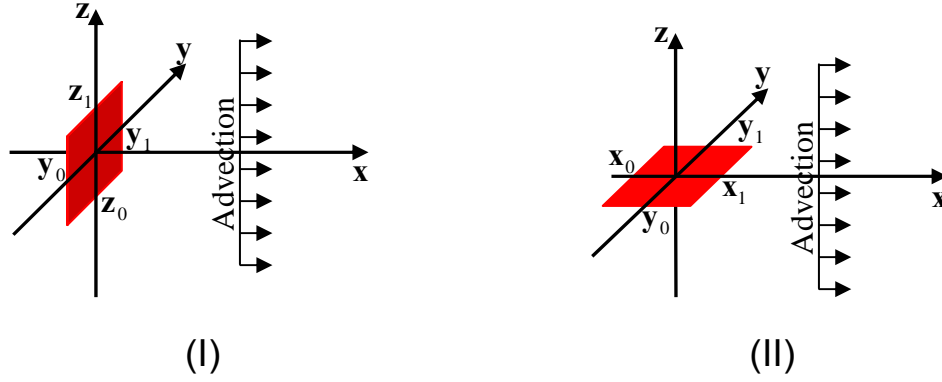
Figure 4-2-4-1 Area source in infinite three-dimensional domain

4.2.4.1 Area source perpendicular to advection direction

The governing equation about the particle concentration is given as,

$$\mathbf{u_t + Vu_x - D(u_{xx} + u_{yy} + u_{zz})} = \begin{cases} \mathbf{q_a\delta(x),} & \text{if} \quad \mathbf{y \in [y_0, y_1]} \quad \text{and} \quad \mathbf{z \in [z_0, z_1],} \\ \mathbf{0,} & \text{otherwise,} \end{cases}$$

$$(4\text{-}2\text{-}4\text{-}1)$$

where $\mathbf{-\infty < x, y, z < \infty}$, $\mathbf{0 < t < \infty}$, $\mathbf{q_a}$ denotes the released particle number in unit area and in unit time.

According to the GFM and applying the property of delta function, the solution is in the form as,

$$\mathbf{u(x, y, z, t) = \int_0^t q_a X(0, \tau; x, t) \int_{y_0}^{y_1} Y(\eta, \tau; y, t) d\eta \int_{z_0}^{z_1} Z(\zeta, \tau; z, t) d\zeta d\tau =}$$

$$\mathbf{= \int_0^t \frac{q_a}{\sqrt{64\pi D\tau}} \exp\left[-\frac{(x - V\tau)^2}{4D\tau} \right] \left[\operatorname{erfc}\left(\frac{y - y_1}{\sqrt{4D\tau}} \right) - \operatorname{erfc}\left(\frac{y - y_0}{\sqrt{4D\tau}} \right) \right] \cdot}$$

$$\mathbf{\cdot \left[\operatorname{erfc}\left(\frac{z - z_1}{\sqrt{4D\tau}} \right) - \operatorname{erfc}\left(\frac{z - z_0}{\sqrt{4D\tau}} \right) \right] d\tau} \qquad (4\text{-}2\text{-}4\text{-}2)$$

The solid curves based on the formula, as shown in Figure 4-2-4-2, stand for the normalized particle concentrations along the $\mathbf{x}$-axis at $\mathbf{t = 1}$s and $\mathbf{t = 2}$s, respectively, if $\mathbf{y_0 = z_0 = -0.5}$ cm and $\mathbf{y_1 = z_1 = 0.5}$ cm. The different symbols are the GASFLOW simulating points, which are coincident with the theoretical curves except slight deviations on some points caused by statistical effects.
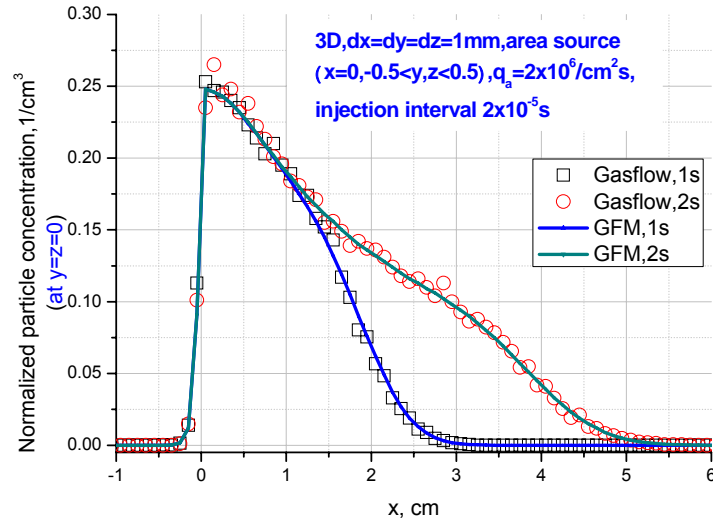
Figure 4-2-4-2 Advection diffusion from continuous particle area source distributed in transverse $(\mathbf{y-z})$ plane in three-dimensional domain

4.2.4.2 Area source parallel to advection direction

For completeness, the equation and the solution are directly given as,

$$\mathbf{u_t + Vu_x - D(u_{xx} + u_{yy} + u_{zz})} = \begin{cases} \mathbf{q_a\delta(z),} & \text{if} \quad \mathbf{x \in [x_0, x_1]} \quad \text{and} \quad \mathbf{y \in [y_0, y_1],} \\ \mathbf{0,} & \text{otherwise,} \end{cases}$$

$$(4\text{-}2\text{-}4\text{-}3)$$

where $-\infty < \mathbf{x, y, z} < \infty$, $0 < \mathbf{t} < \infty$. The solution can be obtained simply,

$$\mathbf{u(x, y, z, t)} = \int_0^{\mathbf{t}} \mathbf{q_a} \int_{\mathbf{x_0}}^{\mathbf{x_1}} \mathbf{X(\xi, \tau; x, t)d\xi} \int_{\mathbf{y_0}}^{\mathbf{y_1}} \mathbf{Y(\eta, \tau; y, t)d\eta Z(0, \tau; z, t)d\tau} =$$

$$= \int_0^{\mathbf{t}} \frac{\mathbf{q_a}}{\sqrt{64\pi\mathbf{D\tau}}} \left[\mathbf{erfc}\left(\frac{\mathbf{x - V\tau - x_1}}{\sqrt{4\mathbf{D\tau}}} \right) - \mathbf{erfc}\left(\frac{\mathbf{x - V\tau - x_0}}{\sqrt{4\mathbf{D\tau}}} \right) \right] \cdot$$

$$\cdot \left[\mathbf{erfc}\left(\frac{\mathbf{y - y_1}}{\sqrt{4\mathbf{D\tau}}} \right) - \mathbf{erfc}\left(\frac{\mathbf{y - y_0}}{\sqrt{4\mathbf{D\tau}}} \right) \right] \mathbf{exp}\left[-\frac{\mathbf{z}^2}{4\mathbf{D\tau}} \right] \mathbf{d\tau} \,. \qquad (4\text{-}2\text{-}4\text{-}4)$$

As an example, the concentration distributions along the line of $\mathbf{y = z = 0.1}$ cm at different times are compared between the theory and the GASFLOW calculations, as shown in Figure 4-2-4-3, where $\mathbf{x_0 = y_0 = -0.5}$ cm and $\mathbf{x_1 = y_1 = 0.5}$ cm. The figure shows good

consistency between the solid lines and the simulating symbols expect slight statistical deviations at some numerical points.
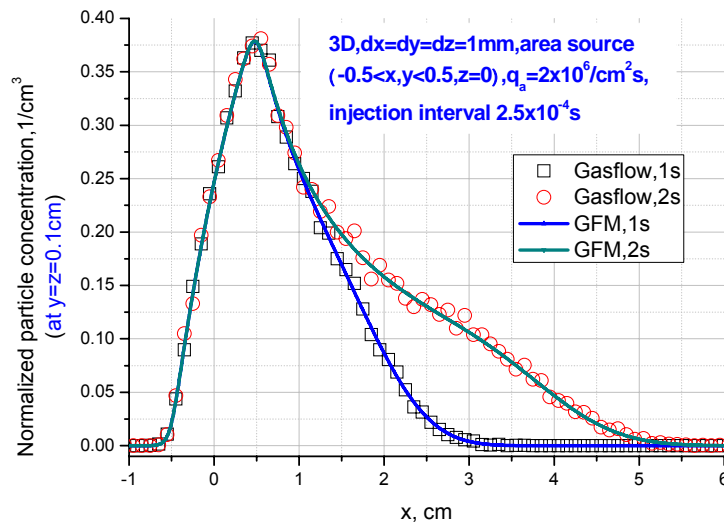

Figure 4-2-4-3 Advection diffusion from continuous particle area source distributed in $x-y$ plane in three-dimensional domain

4.2.5 Volumetric source in three-dimensional advective flow

As the last case, the advection diffusion from a cube of particle source in a 3D domain is considered, as shown in Figure 4-2-5-1.
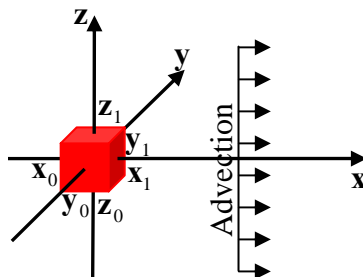

Figure 4-2-5-1 Volume source in infinite three-dimensional domain

The mathematical description of the problem is,

$$\mathbf{u_t} + \mathbf{Vu_x} - \mathbf{D}(\mathbf{u_{xx}} + \mathbf{u_{yy}} + \mathbf{u_{zz}}) = \begin{cases} \mathbf{q_v}, & \text{if} \quad \mathbf{x} \in [\mathbf{x_0}, \mathbf{x_1}], \quad \mathbf{y} \in [\mathbf{y_0}, \mathbf{y_1}] \quad \text{and} \quad \mathbf{z} \in [\mathbf{z_0}, \mathbf{z_1}], \\ 0, & \text{otherwise,} \end{cases}$$

(4-2-5-1)

- 34 -

where $-\infty < x, y, z < \infty$, $0 < t < \infty$, q_v stands for the number of particles released in unit volume and in unit time. The solution is expressed as, according to the GFM,

$$u(x,y,z,t) = \int_0^t q_v \int_{x_0}^{x_1} X(\xi,\tau;x,t)d\xi \int_{y_0}^{y_1} Y(\eta,\tau;y,t)d\eta \int_{z_0}^{z_1} Z(\zeta,\tau;z,t)d\zeta d\tau =$$

$$= \int_0^t \frac{q_v}{8} \left[\mathrm{erfc}\left(\frac{x - V\tau - x_1}{\sqrt{4D\tau}} \right) - \mathrm{erfc}\left(\frac{x - V\tau - x_0}{\sqrt{4D\tau}} \right) \right] \cdot$$

$$\cdot \left[\mathrm{erfc}\left(\frac{y - y_1}{\sqrt{4D\tau}} \right) - \mathrm{erfc}\left(\frac{y - y_0}{\sqrt{4D\tau}} \right) \right] \left[\mathrm{erfc}\left(\frac{z - z_1}{\sqrt{4D\tau}} \right) - \mathrm{erfc}\left(\frac{z - z_0}{\sqrt{4D\tau}} \right) \right] d\tau . \quad (4\text{-}2\text{-}5\text{-}2)$$

Figure 4-2-5-2 depicts the comparison between the Green's function solution and the GASFLOW simulations, while $x_0 = y_0 = z_0 = -0.5$ cm and $x_1 = y_1 = z_1 = 0.5$ cm. As can be seen from the figure, the concentrations along the x-axis, i.e., the advection direction, agree to each other between the theory and the numerical calculation at the different times.
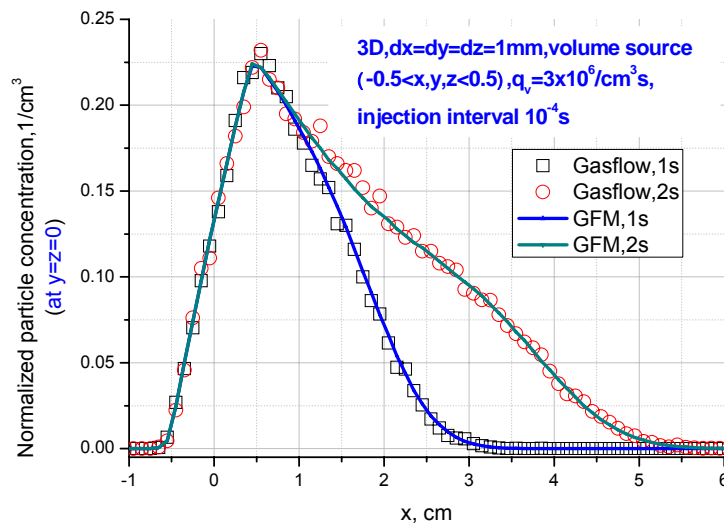

Figure 4-2-5-2 Advection diffusion from continuous particle volume source in three-dimensional domain

The series of quantitative validation calculations in Section 4.2.1 through 4.2.5 prove that the models of the particle transport and the particle dispersion in GASFLOW can reproduce effectively the physical phenomena in a numerical way.

5. Simulation of FZK dust dispersion tube with air injection

An experimental facility has been constructed in Forschungszentrum Karlsruhe (FZK) to study the dust mobilization provoked by air injected through the holes of a cylindrical tube situated at the bottom of another bigger one where a dust layer has been situated. The scheme of the dispersion tube is depicted in Figure 5-1.
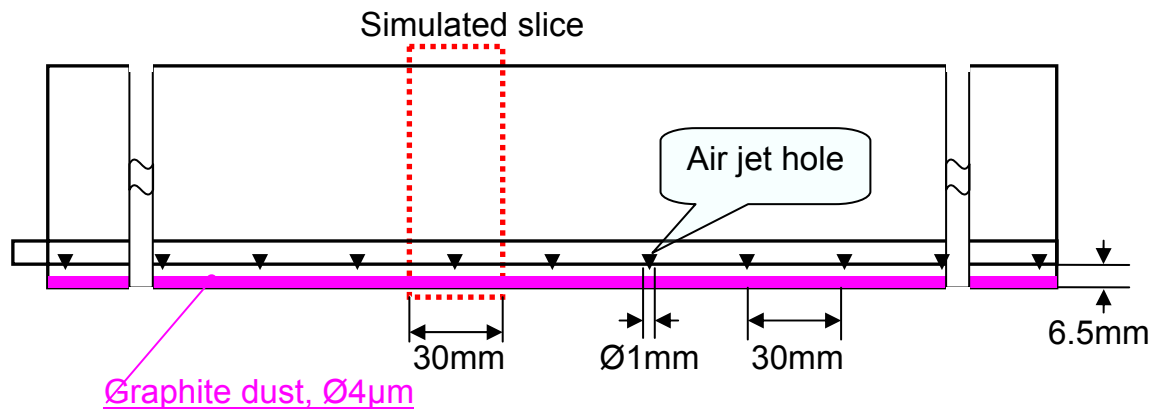

Figure 5-1 FZK dust dispersion tube geometry

The primary parameter settings are the inner diameter of the bigger tube 150 mm, the inner / external diameter of the smaller tube is 12 / 14 mm, graphite dust particle diameter 4 microns, the closest distance between the two tubes is 6.5 mm. The air is injected through a host of small holes with a diameter of 1 mm, which are drilled on the bottom of the smaller tube with an interval of 30 mm. The rest pressure of the bigger tube is 0.6 bar, the air injection pressure is 21 bar, and the injection lasts 130 ms.

Only a section of 30 mm of the tubes with only one injection hole in the middle is modeled in the GASFLOW simulations. A cylindrical computational grid containing 15 x 29 x 13 cells is set up, 15 cells in the radius direction, 29 cells in the azimuth direction, and 13 cells in the axis direction. The none-uniformed cells are adaptively distributed in the computational domain.

It is actually a sonic flow occurring at the injection holes, according to a theoretical calculation, based on which the critical flow velocity is 317 m/s and the critical pressure 11 bar. Then a velocity boundary is applied for the jet hole in the GASFLOW simulations. Thus the gas dynamics in the smaller tube is not modeled. The boundary conditions on any solid walls are assumed to be free-slip.

The k-epsilon turbulence model is adopted in the simulations. Symmetric boundary conditions are applied at the two cross-ends of the simulated section.

The transient process of the dust dispersion is simulated by GASFLOW. The computed dust cloud at 35 ms later than the starting point of the injection is shown as the right picture in Figure 5-2. Accordingly the left one is the experimental dust cloud at the same moment recorded by a camera. The similar behavior of the dust cloud can be seen roughly based on the two pictures.
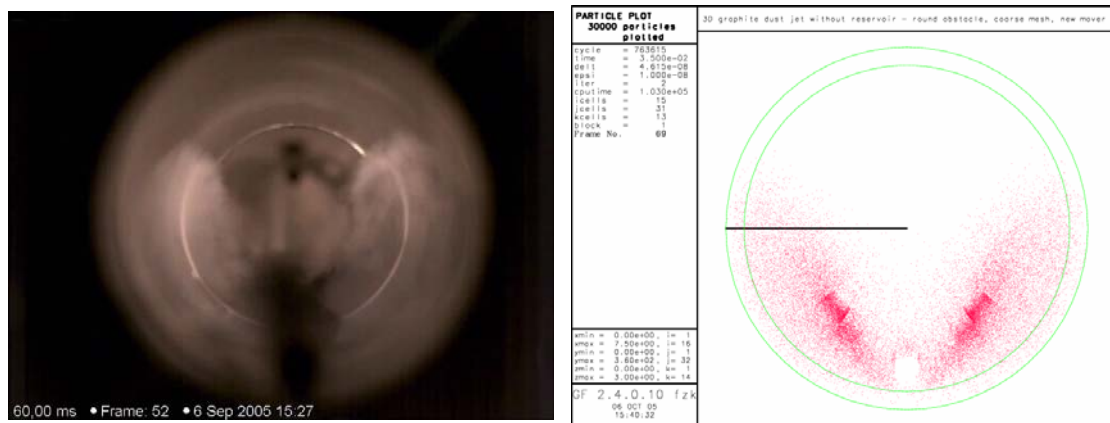

Figure 5-2 Experimental and numerical dust clouds at 35 ms after starting injection of strong air flow, which blows up the graphite dust on the bottom of the dispersion tube in FZK

To compare quantitatively the experiment and the numerical simulation, an angle of the dust cloud front is defined, as shown in Figure 5-3 (a). The time-history of developing process of the dust cloud front angel is shown in Figure 5-3 (b). According to the figure, the experimental dust cloud grows slower than the simulation before about 30 ms. This is maybe caused by that the injection sonic flow in the experiment needs some time to grow from zero mass flow rate to the critical flow rate. However, in the numerical simulation, the increasing of the mass flow rate is like the behavior of the Heaviside function, just a jump without any time delay. If this factor is considered, GASFLOW could produce better results.

(a)
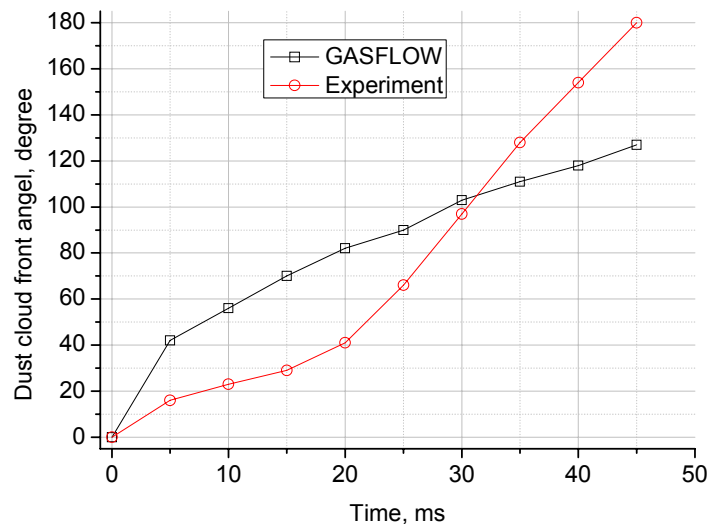
(b)

Figure 5-3 Definition of dust cloud front angel (a) and its time-history (b)

6. Conclusions

Based on the computational fluid dynamics computer code GASFLOW, a discrete Lagrangian particle model has been defined and reviewed, including the governing equation system of particle transport, the turbulent particle dispersion model and the modeling of particle/boundary interactions, like the particle deposition/rebound model with a definition of the threshold bounce velocity, the particle entrainment model with the semi-empirical

threshold particle suspension velocity, and the particle cloud model and so on.

The particle transport model is validated by the test cases of particle mobilizations in uniform advective flows in a rectangular and a curved duct, respectively, without considering the particle dispersions. The high agreements between the analytical particle trajectories and the computed trajectories manifest that the governing equations of particle motion are solved correctly.

Two test cases of particle mobilization problems in a straight and a curved duct are solved, respectively, by switching on the particle dispersion models. The simulations indicate that the lighter particle cloud spreads more than the heavier when the same level of turbulence occurs in both cases. It is certain that the dust cloud disperses more if the turbulent intensity is enhanced.

Based on the theoretical Green's function solutions, a series of particle mobilization problems in three-dimensional advective flows are simulated and compared to the analytical solutions. The particle sources are assumed to be instantaneous /continuous, point /line /area /volumetric, and are released into quiescent fluid or advective flows. Very good consistencies are found between the GASFLOW simulations and the theory when the Reynolds number based on the particle diameter is much less than unit, namely, when the drag force of the flow on the particle sphere satisfies the Stoke's law. These validations have verified both the particle motion model and the particle dispersion model.

The graphite dust dispersion experiment performed in Forschungszentrum Karlsruhe is simulated by GASFLOW. The computed dust cloud developing process is compared to the recorded dust clout dispersion process in the experiments. It can be concluded that the GASFLOW simulations produced quite satisfactory results both qualitatively and quantitatively.

The direction of the future work would be moved from validation of the particle transport towards the verification of the particle deposition and re-suspension.

Acknowledgments

framework of the European Fusion Development Agreement. The views and opinions expressed herein do not necessarily reflect those of the European Commission.

REFERENCES

[1] Barkhudarov, M., Ditter, J.L., Particle Transport and Diffusion, Flow Science, Inc., August 1994.

[2] Xu, Z., Breitung, W., Travis, J.R., Necker G., Development and validation of particle transport and diffusion models for dust explosion simulation in ITER, Annual Meeting on Nuclear Technology, Karlsruhe, Germany, May 2007.

[3] Francisco J. Cabrejos and George E. Klinzing, "Incipient Motion of Solid Particles in Horizontal Pneumatic Conveying," Dept. of Mech. Engr., University of Pittsburgh, unpublished paper (1991).

[4] Travis, J.R. et al., "GASFLOW-II: A Three Dimensional Finite-Volume Fluid Dynamics Code for Calculating the Transport, Mixing and Combustion of Flammable Gases and Aerosols in Geometrically Complex Domains, Vol. 1: Theory and Computational Model, Vol. 2: User's Manual, Vol. 3: Assessment Manual", Bericht FZKA-5994, LA-13357-M, Oktober 1998.

[5] Kay, A., Advection-diffusion in reversing and oscillating flows: 1. the effect of a single reversal, IMA Journal of Applied Mathematics (1990) 45, 115-137.

[6] Leij, F.J., Priesack, E., Schaap, M.G., Solute transport modeled with Green's functions with application to persistent solute sources, Journal of Contaminant Hydrology 41 (2001) 155-173.

[7] Leij, F.J., van Genuchten, M.T., Analytical modeling of non-aqueous phase liquid dissolution with Green's functions, Transport in Porous Media 38: 141-166, 2000.

[8] Lin, J.S., Hildemann, L.M., Analytical solutions of the atmospheric diffusion equation with multiple sources and height-dependent wind speed and eddy diffusivities, Atmospheric Environment Vol. 30, No. 2, pp. 239-254, 1996.

[9] Park, E., Zhan, H., Analytical solutions of contaminant transport from finite one-, two-, and three-dimensional sources in a finite-thickness aquifer, Journal of Contaminant Hydrology 53 (2001) 41-61.

[10] Duffy, D.G., Green's Functions with Applications, Chapman & Hall/CRC, 2001.

[11] Greenberg, M.D., Application of Green's Functions in Science and Engineering, Prentice-Hall, Inc., Englewood Cliffs, New Jersey, 1971.

[12] Beck, J.V., Cole, K.D., Haji-Sheikh, A., Litkouhi, B., Heat Conduction Using Green's Functions, Hemisphere Publishing Corporation, 1992.

[13] Xu, Z., Travis, J.R., Breitung, W., Green's function method and its application to benchmark verifications of diffusion models of GASFLOW code, FZKA report 7292, Forschungszentrum Karlsruhe, January 2007.